



HAL
open science

Upgrade and extension of LSA-SAF land surface albedo archive from EPS Metop/AVHRR: description and quality assessment

Anthéa Delmotte, Daniel Juncu, Xavier Ceamanos, Isabel F Trigo, Sandra Gomes

► To cite this version:

Anthéa Delmotte, Daniel Juncu, Xavier Ceamanos, Isabel F Trigo, Sandra Gomes. Upgrade and extension of LSA-SAF land surface albedo archive from EPS Metop/AVHRR: description and quality assessment. *European Journal of Remote Sensing*, 2024, Article: 2300043, pp.1–28. 10.1080/22797254.2023.2300043 . hal-04425531

HAL Id: hal-04425531

<https://hal.science/hal-04425531>

Submitted on 30 Jan 2024

HAL is a multi-disciplinary open access archive for the deposit and dissemination of scientific research documents, whether they are published or not. The documents may come from teaching and research institutions in France or abroad, or from public or private research centers.

L'archive ouverte pluridisciplinaire **HAL**, est destinée au dépôt et à la diffusion de documents scientifiques de niveau recherche, publiés ou non, émanant des établissements d'enseignement et de recherche français ou étrangers, des laboratoires publics ou privés.



Distributed under a Creative Commons Attribution 4.0 International License



Upgrade and extension of LSA-SAF land surface albedo archive from EPS Metop/AVHRR: description and quality assessment

Anthéa Delmotte, Daniel Juncu, Xavier Ceamanos, Isabel F. Trigo & Sandra Gomes

To cite this article: Anthéa Delmotte, Daniel Juncu, Xavier Ceamanos, Isabel F. Trigo & Sandra Gomes (21 Jan 2024): Upgrade and extension of LSA-SAF land surface albedo archive from EPS Metop/AVHRR: description and quality assessment, European Journal of Remote Sensing, DOI: [10.1080/22797254.2023.2300043](https://doi.org/10.1080/22797254.2023.2300043)

To link to this article: <https://doi.org/10.1080/22797254.2023.2300043>



© 2024 The Author(s). Published by Informa UK Limited, trading as Taylor & Francis Group.



Published online: 21 Jan 2024.



Submit your article to this journal [↗](#)



Article views: 112



View related articles [↗](#)



View Crossmark data [↗](#)

Upgrade and extension of LSA-SAF land surface albedo archive from EPS Metop/AVHRR: description and quality assessment

Anthéa Delmotte^a, Daniel Juncu^a, Xavier Ceamanos^a, Isabel F. Trigo^b and Sandra Gomes^b

^aCNRM, Météo-France, CNRS, Université de Toulouse, Toulouse, France; ^bInstituto Português do Mar e da Atmosfera (IPMA), Lisbon, Portugal

ABSTRACT

ETAL is the operational EPS Ten-Day Albedo product, produced by the EUMETSAT Satellite Application Facility for Land Surface Analysis (LSA SAF). By back-processing the full catalogue of EPS-Metop radiance data from September 2007 to June 2021, we are able to 1) extend the temporal coverage (previously the archive only went back to 2015) and 2) improve the product archive that was based on near-real time (NRT) processing; the second point is achieved by using reanalyses instead of forecasts of atmospheric conditions and by not being exposed to missing data in the NRT radiance inputs. We present this reprocessed part of the ETAL data set, called ETAL-R, and assess its quality and consistency with respect to the original archive of NRT ETAL data (for the overlapping period 2015–2021), as well as its accuracy compared to albedo from MODIS and ground stations. ETAL-R exhibits reliable long-term stability and increased homogeneity compared to the NRT archive, and the comparison against the additional reference data shows satisfactory accuracy. Overall, ETAL-R is shown to be very consistent with the ETAL NRT archive while – under certain circumstances – improving it.

ARTICLE HISTORY

Received 3 December 2022
Revised 19 November 2023
Accepted 22 December 2023

KEYWORDS

Surface albedo; AVHRR;
Metop; LSA-SAF; EUMETSAT

Introduction

Land surface albedo is the ratio of reflected to incoming solar radiation at the Earth's surface. This variable was declared an Essential Climate Variable by the Global Climate Observing System (WMO, 2011) because long-term observations give essential information on the surface radiation budget and are closely linked to climate change. The evolution of land surface albedo is an indicator of deforestation, desertification and melting ice, for example (Becerril-Piña et al., 2016; Dirmeyer & Shukla, 1994; Riihelä et al., 2013).

Its monitoring through satellite observations is therefore important as it allows dense spatial coverage for the whole Earth, allowing us to constrain climate-related changes on the Earth's surface over prolonged time intervals. Surface albedo is also an important variable for Numerical Weather Prediction (NWP) due to its impact on surface temperature and net radiation (Cedilnik et al., 2012).

The main mission of the EUMETSAT (European organization for the Exploitation of Meteorological Satellites) Satellite Application Facility on Land Surface Analysis (LSA-SAF) is to derive land surface variables, including surface albedo, from EUMETSAT satellites. Examples are the geostationary Meteosat

satellites and the polar orbiting series of Metop satellites of the European Polar System (EPS). Instruments on board Metop-A (launched on 19 October 2006), Metop-B (launched on 17 September 2012) and Metop-C (launched on 7 November 2018) satellites allow to observe the Earth by day and night, under cloudy conditions, to get data for both operational meteorology and climate studies. It is the case of the Advanced Very High Resolution Radiometer (AVHRR), onboard each Metop satellites, which covers the full globe and generates data on which the Near-Real Time (NRT) EPS Ten-day Albedo (ETAL; Lellouch et al., 2020) is based. ETAL provides maps of surface albedo every 10 days that are freely available through the LSA-SAF website. Lellouch2020 found these data to be accurate with respect to *in situ* measurements of surface albedo and the satellite product derived from the MODerate resolution Imaging Spectroradiometers (MODIS; Schaaf et al., 2002). Current applications of ETAL include its use in the production of downstream LSA-SAF vegetation products.

While NRT products are crucial for NWP and other time-constrained applications, it can sometimes be useful (for climate-related studies, for example) to generate back-processed data sets which are more homogeneous and consistent. We

have done so in the case of ETAL by using reanalyses instead of forecasts of atmospheric composition as well as the complete archive of Metop-AVHRR radiance observations, with occasional data gaps having been filled. Because the operational production of ETAL only started on 25 January 2015 (meaning that the current archive of ETAL data does not go back further than that) by using the complete catalogue of radiances allows us to extend the ETAL archive further back in time. The reprocessed ETAL data set, which we call ETAL-R, covers the time period from 25 January 2007 to 30 June 2021 and will be made available to users following an internal review process. Apart from the differences in input data temporal coverage, the retrieval algorithm to obtain ETAL-R is the same that has been used to retrieve the NRT ETAL data.

The aim of this article is to present ETAL-R as well as extensively assess its accuracy. In order to do so, we follow four steps:

- First, we quantify the differences of ETAL-R with respect to the NRT-processed ETAL archive, for the full global domain over a six-year period (2015–2020) with more detailed seasonal and latitudinal comparisons.
- Second, we assess the completeness and stability of ETAL-R.
- Third, we use reference measurements of surface albedo from ground stations and MODIS for additional evaluation on accuracy, uncertainty, and precision of the satellite products.
- Finally, we showcase data from the Sahel region in Africa for the full ETAL-R time coverage to illustrate how this data set can be used to highlight and investigate spatial and temporal changes of surface albedo due to environmental conditions.

Data

Definitions of surface albedo

Two definitions of surface albedo can be distinguished depending on the illumination conditions: white-sky and black-sky albedo (Schaepman-Strub et al., 2006).

- White-sky albedo (WSA) corresponds to bi-hemispherical (BH) reflectance and diffuse illumination conditions, which can be explained by scattering of solar radiation by aerosols in the atmosphere.
- Black-sky albedo (BSA) corresponds to directional-hemispherical (DH) reflectance and direct illumination conditions, thus depending on sun position.

The real-world surface albedo, or blue-sky albedo, is a linear combination of both albedo definitions, depending on the proportion of direct to diffuse radiation. While blue-sky albedo can be directly measured at the ground, satellites can only derive WSA and BSA after integrating the surface bi-directional reflectance distribution function (BRDF) that is commonly estimated from a set of multi-angular measurements. For most results reported in this work, only the analysis of WSA will be given in the core of this document, while the results for BSA will be detailed in [Appendix A](#). The results for the ground stations comparison include both WSA and BSA as it depends on availability of valid data points.

Broadband albedo values are available in three domains: visible (VIS; [0.4 μm -0.7 μm]), near-infrared (NIR; [0.7 μm -4.0 μm]) and total shortwave (BB; [0.3 μm -4.0 μm]). We chose to focus on the total shortwave domain, as it is the most used albedo product by NWP models and because solar radiation is distributed throughout the shortwave spectrum (Liu et al., 2012). Future work may focus on the detailed assessment of the VIS/NIR albedo variables.

Satellite products

ETAL and ETAL-R

The near-real time (NRT) generated ETAL product, derived from AVHRR sensor on board Metop-B, and the reprocessed ETAL-R data, derived from AVHRR sensor on board Metop-A until the end of 2014, and then Metop-B from 2015 onwards, are generated using the same retrieval algorithm (Geiger et al., 2008; Lellouch et al., 2020) and, as such, the obtained data have many characteristics in common, albeit a few differences exist. For ETAL in general, the surface albedo data are produced approximately every 10 days (on the 5th, 15th and 25th of each month) at a ground resolution of 1.1 \times 1.1 km on a sinusoidal projection centred at (0°N, 0°W) and over the full globe. Both types of processing use the preceding 20-day observations, averaged with a weighting approach with maximum weight on the last observation of the composition period. The main differences between ETAL-R and the NRT-generated version are in the input data used and the temporal coverage, which extends back to 25 January 2007 for ETAL-R (compared to 25 January 2015 in the NRT-ETAL archive). Due to limitations in the data calibration of AVHRR (e.g. lack of characterization of temporal drifts), ETAL-R was generated considering that the sensors on Metop-A and Metop-B shared the same spectral response functions during the whole

Table 1. Characteristics of near-real time ETAL data and the reprocessed ETAL-R in terms of sensor, area coverage, resolution and input data. Atmospheric composition inputs refer to mean sea level pressure, total column water vapour and total column ozone.

Data generation	Satellite	Sensor	Temporal Coverage		Spatial Coverage
			Metop-A	Metop-B	
Reprocessing (ETAL-R) Near-real time	Metop-A and B Metop-B	AVHRR	2007/01/25–2014/12/31	2015/01/01–2021/06/30 2015/01/25 – Now	Global
Data generation	Channels (central wavelengths)	Spatial Resolution	Temporal Resolution		Atmospheric Composition Inputs
Reprocessing (ETAL-R) Near-real time	0.6 μ m, 0.8 μ m, 1.6 μ m	1.1 \times 1.1 km	5 th , 15 th & 20 th of each month		ERA5 reanalyses ECMWF forecasts

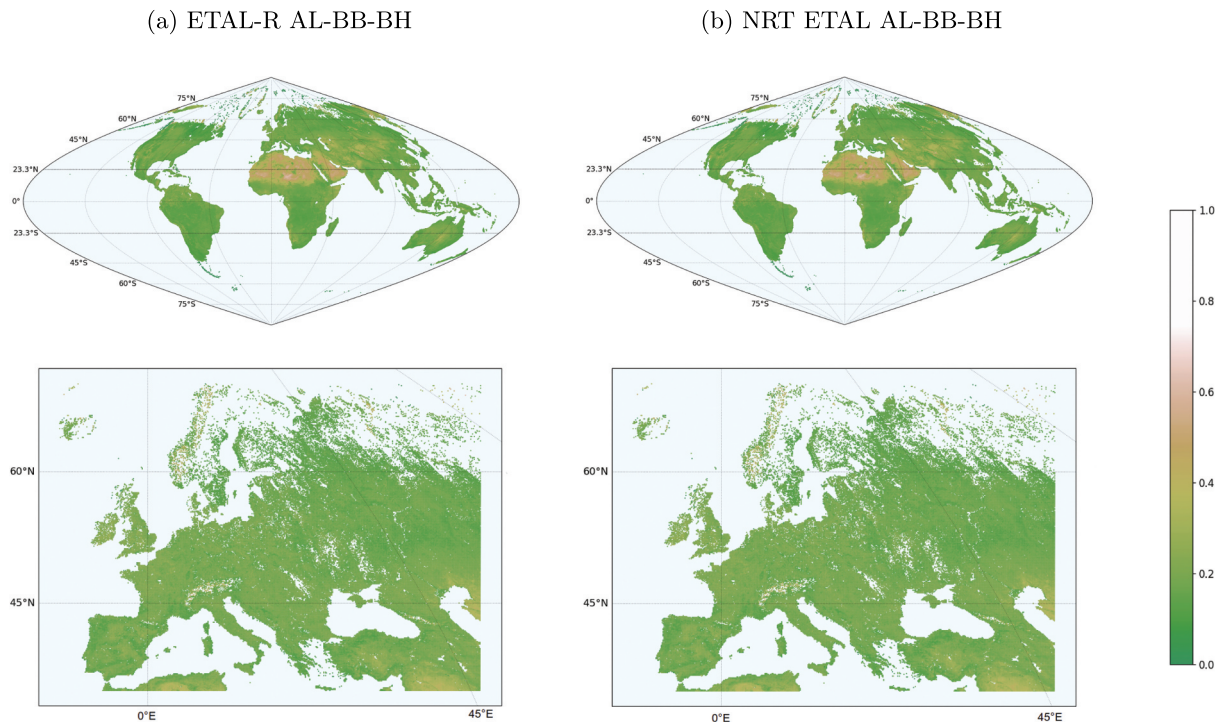


Figure 1. (a) ETAL-R and (b) NRT-generated ETAL AL-BB-BH on 5th June 2021, on a global scale and with a zoom on Europe.

period covered by the data record. The latest Metop-B spectral response functions were chosen as the reference for the sake of consistency with respect to NRT-ETAL (purely based on Metop-B). A similar strategy was satisfactorily considered for other LSA-SAF albedo data records, including the one resulting from the back-processing of the SEVIRI data acquired by 4 different Meteosat Second Generation (MSG) satellites and considering MSG-4 as reference (Carrer et al., 2018).

Once ETAL-R is released it will become the primary LSA SAF AVHRR albedo product for the overlapping period. Table 1 summarizes the main characteristics of ETAL-R and NRT ETAL, as well as center wavelengths of channel of the AVHRR sensor, and Figure 1(a,b) shows global and zoomed maps of AL-BB-BH from ETAL-R and NRT-generated ETAL on 5 June 2021. The AL-BB-DH maps are available in Appendix A.

For both ETAL-R and the NRT-generated ETAL, top of atmosphere (TOA) radiances acquired by the AVHRR instrument aboard the Metop satellites

For both ETAL-R and the NRT-generated ETAL, top of atmosphere (TOA) radiances acquired by the AVHRR instrument aboard the Metop satellites are filtered for clear-sky conditions and atmospherically corrected to retrieve top of canopy (TOC) reflectance values. Atmospheric correction is made using ECMWF (European Centre for Medium-Range Weather Forecasts) forecasts of meteorological atmospheric variables for ETAL NRT processing (<https://www.ecmwf.int/en/forecasts>), while ECMWF ERA-5 reanalyses were used to reprocess the same radiance inputs to obtain ETAL-R (Hersbach et al., 2021). Atmospheric variables correspond to mean sea level pressure, total column water vapour, and total column ozone. Both NRT ETAL and ETAL-R used the same aerosol inputs, which come from a climatology based

upon ECMWF reanalyses as described in Lellouch et al. (2020). Cloud masks, which are generated using the software from the Satellite Application Facility on Support to Nowcasting and Very Short Range Forecasting (<https://www.nwcsaf.org/>) in both cases, were reprocessed for the generation of ETAL-R to correct some dates with corrupted cloud data in the NRT chain. AVHRR input radiances were also revised for completeness and radiometric quality. Using TOC reflectances accumulated over the 20-day period, the parameters of the BRDF can be determined for each pixel by inversion. Surface albedo values for each AVHRR-observed spectral channel are obtained through angular integration of the BRDF parameters. Finally, we determine broadband albedo values through linear conversion of the channel-specific albedo values. BRDF parameter estimates from preceding time slots serve as *a priori* information using a Kalman filter. That allows to reduce data gaps due to cloudy conditions for more consistency in the results. A more detailed description of the algorithm used to retrieve surface albedo from Metop is given in the project documentation (LSA-SAF, 2018a) and in Lellouch et al. (2020).

The dataset structure for all disseminated ETAL files is as follows: broadband albedo files contain 4 albedo quantities (BH and DH both for BB, DH for NIR and DH for VIS), their respective uncertainty estimates (ERR), the quality flag (Q-Flag), and the “age” of the information (Z_{age}) (LSA-SAF, 2018b). Spectral albedo for all three AVHRR channels are also made available to users. All of these products are provided in the HDF5 format (also available in a regular $0.01^\circ \times 0.01^\circ$ grid in NetCDF4) and available on the LSA SAF web portal: <http://lsa-saf.eumetsat.int>. We only use the data variables corresponding to WSA (data variable AL-BB-BH) and BSA (data variable AL-BB-DH) in the total shortwave domain, combined with their covariance error (i.e. data variables AL-BB-BH-ERR and AL-BB-DH-ERR). To ensure the quality of the data, each product is filtered: for both WSA and BSA, pixels are removed if the error of covariance C_k is greater than 10% of the albedo value (Lellouch et al., 2020).

MODIS

MODIS surface albedo products, which are derived from satellites Terra and Aqua, are considered a standard to assess other satellite albedo data (Schaaf et al., 2002). The accuracy of MCD43 products is reported as below 5% for the majority of the validation sites and below 10% for those with low quality flags (<https://modis-land.gsfc.nasa.gov/ValStatus.php?ProductID=MOD43>). We consider variables *MODIS Albedo Black-Sky Albedo Shortwave Daily L3 Global 30 ArcSec CMG* (MCD43D51 v006) and *MODIS Albedo White-Sky Albedo Shortwave Daily L3 Global 30 ArcSec CMG* (MCD43D61 v006) for land surface albedo comparison and *MODIS Albedo QA BRDF Quality Daily L3 Global 30 ArcSec CMG* (MCD43D31 v006) as quality flags to filter the two previous albedo data sets. All of these products are generated for the full globe, on a daily basis using 16 days of Terra and Aqua observations and projected on a equirectangular grid with 30 arc seconds (i.e. 0.0083°) resolution.

The two land surface albedo products are filtered depending on their BRDF quality. Albedo pixels are removed when BRDF Albedo Quality Flag $\neq 0$ in MCD43D31 product. As MODIS is only used for local analysis in this study, albedo values are calculated for the nearest pixel to ground stations in case of comparison with one of them, or averaged over an area of 10×10 pixels when no stations exist, based on the ETAL-R closest pixel. We compare all products based on ETAL-R available dates (the 5th, 15th and 25th of each month), by maximizing the overlap in number of days between the 16-day composite period of MODIS and the 20-day composite period of ETAL-R.

Ground observations

ETAL-R is also compared to ground station observations from three different networks, namely BSRN (Baseline Surface Radiation Network; <https://bsrn.awi.de/>; Driemel et al., 2018), AmeriFlux (<https://ameriflux.lbl.gov/>) and GBOV project (Ground-Based Observations for Validation of Copernicus Global Land Products; <https://gbov.acri.fr/>). Cumberland Plain (CUMB), Gobabeb (GOB; Vogt,

Table 2. List of ground stations and their characteristics. Hyphens are for missing information.

Station	Country	Position		Tower Height	Footprint	Surface type	Network
		Lat	Lon				
Gobabeb	GOB	Namibia	−23.5195	15.0832	2m	25.24m	BSRN
Morgan Monroe State Forest	MMS	USA	39.3232	−86.4131	48m	606.10m	Deciduous Broadleaf
Table Mountain	TBL	USA	40.1249	−105.2368	10m	126.20m	Barren
Cumberland Plain	CUMB	Australia	−33.6150	150.7230	–	–	Evergreen Broadleaf
Payerne	PAY	Switzerland	46.8150	6.9440	2m	25.24m	Croplands
Tateno	TATE	Japan	36.0592	140.1244	2m	25.24m	Urban and Built-up

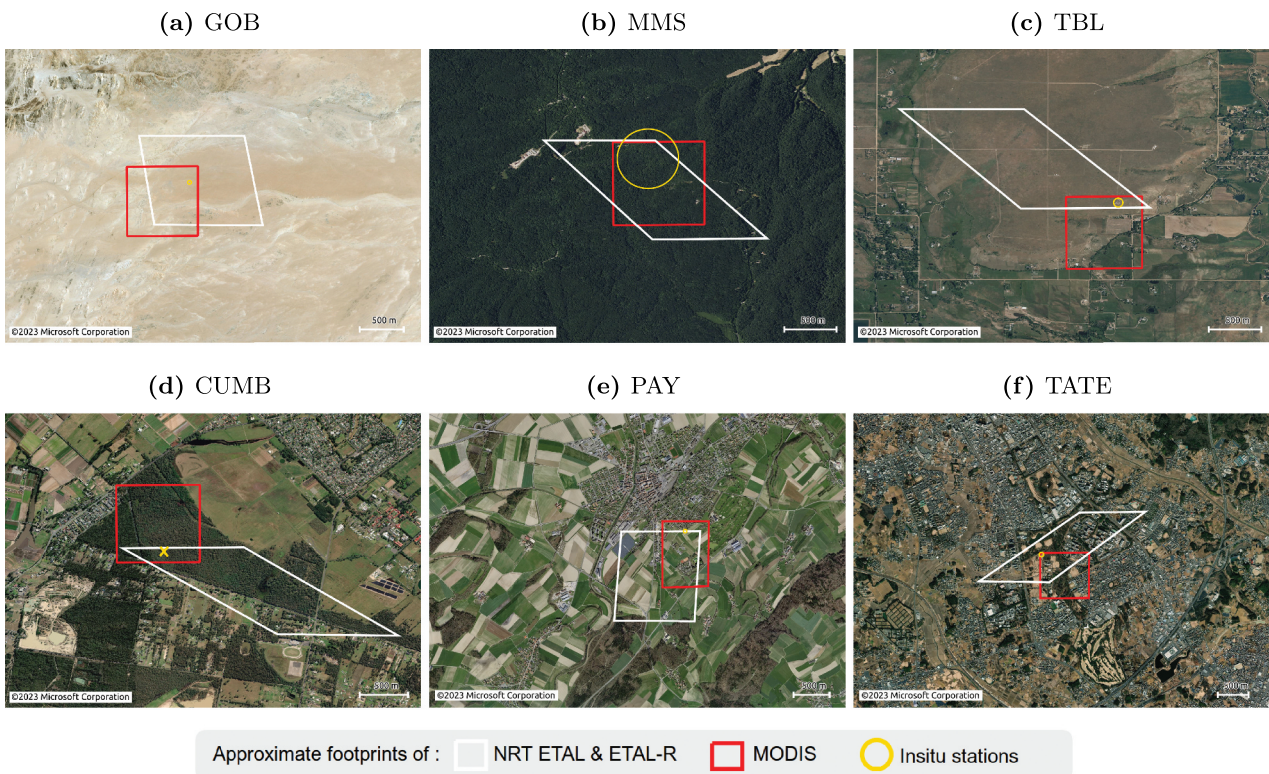


Figure 2. Ground stations and their ETAL and MODIS approximate footprints. Stations whose footprint could not be calculated are identified by a cross.

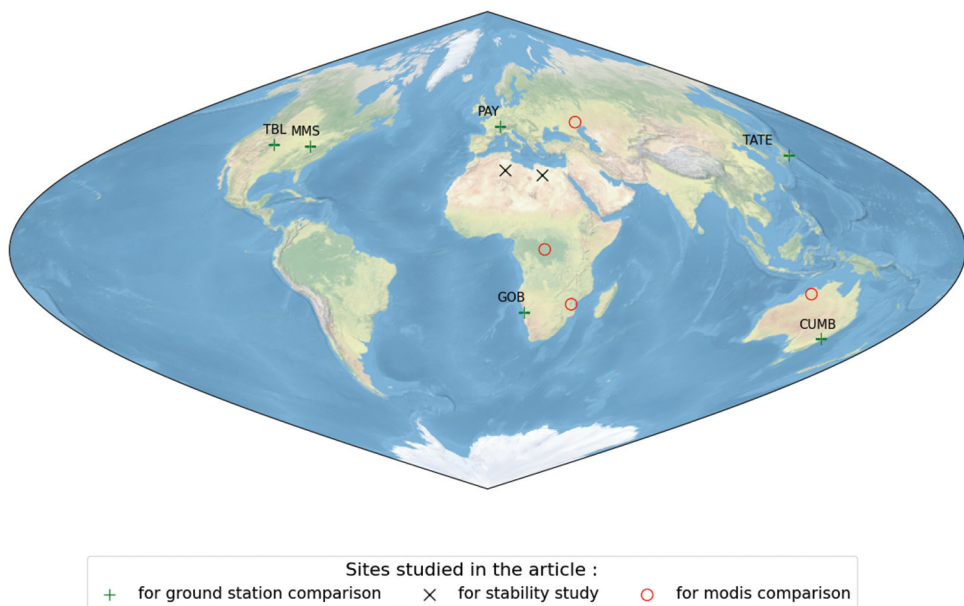


Figure 3. Location of ground stations and sites considered in this study. Basemap from natural earth (naturalearthdata.com).

2021), Morgan Monroe State Forest (MMS; Novick & Phillips, 2022), Payerne (PAY; Vuilleumier, 2021), Table Mountain (TBL), and Tateno (TATE) stations were selected for the evaluation against *in situ* measurements (see Table 2 for details on their location and surface type). The footprint of each station is calculated based on the height of the tower accord-

ing to the formula described by Wang et al. (2019). The high-resolution satellite images from the Maxar constellation and the approximate satellite pixels used for comparison are given in Figure 2, while their location on global map are given in Figure 3. These stations were chosen for their variability of land covers and latitudes, the visual homogeneity of

their satellite footprint and their availability over a long period of time, more specifically the 2017–2020 period. The sites are located all around the globe and represent five different types of land cover. We have chosen three stations for which the satellite footprints were found to be homogeneous in terms of landscape to be consistent with the ground station footprint, i.e. GOB, MMS, and TBL. Three other stations with a more heterogeneous satellite footprint, i.e. CUMB, PAY, and TATE, were also selected due to the low number of stations meeting our criteria of temporal availability (2017–2020) and spatial representativeness (Román et al., 2009; Wang et al., 2019). In particular, PAY and TATE allow us to highlight the limits of ground stations close to urban areas. The satellite footprint of CUMB is also heterogeneous but with a majority of surrounding forests.

Depending on the network, temporal resolution varies from 1 to 3 min for BSRN, 1 min to 1 h for GBOV and 1 day for AMERIFLUX. Blue-sky surface albedo is calculated for each station from the ratio of shortwave up-welling (SWU) and down-welling (SWD) radiation measurements and then averaged to produce a daily product, when time

resolution is lower than 1 day. BSA and WSA are derived from blue-sky albedo, using diffuse radiation measured at the stations. This method, defined by Kharbouche et al. (2019) and applied by Juncu et al. (2022) for example, consists in removing data whenever the ratio of diffuse radiation and SWD is above (or below) a defined threshold to estimate WSA (or BSA). Here, the threshold values are, respectively, 0.99 and 0.1 for WSA and BSA.

Based on the quantity of valid data points, we compare BSA for GOB and CUMB, blue-sky albedo for MMS (because diffuse radiation is not provided for AMERIFLUX stations) and WSA for TBL, TATE, and PAY. These stations show different types of land cover, such as barren, cropland, deciduous broadleaf, evergreen needleleaf, and evergreen broadleaf forests. Even though the surface type of GOB and TBL is the same, they do not present the same features. The first one corresponds to desert gravel, while the second is more sandy, with a mix of exposed rocks and sparse grass (see Figure 2). To keep only the significant data, SWD radiation flux over the day was discarded whenever they drop below 50 W.m^{-2} , are null or negative, and then averaged on a daily product. Data acquired with solar zenith angle larger than 75° were removed too. As ground observations are available on a daily basis, they were averaged over the 20 days previous to the date of each ETAL product (5th, 15th or 25th).

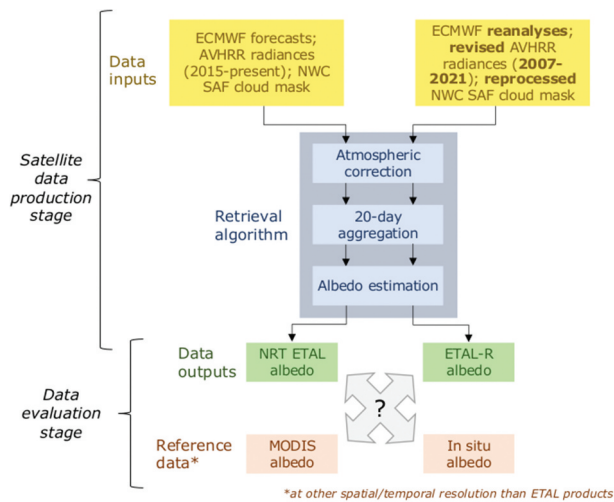


Figure 4. Scheme of the data processing regarding ETAL-R and NRT-ETAL and their comparison with reference data.

Validation protocol

The scheme in Figure 4 summarizes the approach applied from data processing to data outputs, and validation. On one side, ECMWF forecasts and AVHRR radiances from 2015 are used as data inputs of the retrieval algorithm, while on the other side, the data inputs contain ECMWF reanalysis with revised AVHRR radiances from 2007 to 2021. The algorithm first applies atmospheric correction on the data, which is then aggregated over

Table 3. Recommended best practices for the validation of surface albedo products from Wang et al. (2019).

Quantity	Recommended practices
Accuracy	Median error Median and percentiles of residuals Box-plots of residuals vs. Albedo
Precision	Median absolute deviation Median 3 point difference
Uncertainty	Scatter plot of match-ups Median and percentiles of absolute residuals, RMSD
Completeness	Box-plots of absolute residuals vs. Albedo Gap size distribution Gap length
Stability	Time series average, standard deviation and regression slope Mean error per decade

Table 4. Accuracy requirements for validation of satellite surface albedo from the PRD of LSA-SAF.

Variable	Horizontal Resolution	Vertical Resolution	Temporal Resolution	Accuracy			
				Threshold	Target	Optimal	
BSA/WSA	1 km	N/A	Daily to weekly	$AL \geq 0.15$	20%	10%	5%
				$AL < 0.15$	0.03	0.015	0.0075

a 20-day window to finally estimate both NRT ETAL and ETAL-R albedo. This section presents the comparisons that are then made between the satellite data and *in situ* measurements of surface albedo.

Recommended practices for validation

The CEOS, the Committee on Earth Observation Satellites (Wang et al., 2019), recommends a set of good practices in order to validate satellite products of surface albedo (see Table 3). The recommended practices in bold in the table are the ones that we chose to apply in our validation protocol. Their implementation is described in Section 3.3.

As described in Wang et al. (2019), accuracy represents the agreement between a measurement and a reference considered as the true value. Other parameters are not based on a reference value. Precision refers to the repeatability of the measurement, i.e. whether the same measurement can be obtained under similar conditions. Uncertainty is the parameter that shows the dispersion due to the measuring device. The completeness characterizes the frequency and continuity of a dataset and the stability highlights the trend of a sufficiently long data set.

Validation metrics and requirements

The following metrics are used to assess accuracy, precision, uncertainty, completeness, and stability of ETAL-R product: root-mean-square deviation (RMSD), mean bias error (MBE), mean absolute error (MAE), median absolute error (MedAE), median of 3-point difference (Med3), standard deviation (STD), and Pearson's correlation coefficient (R). The definition of these criteria is given in Appendix B and a distinction is made between albedo values lower and higher than 0.15, relative metrics being used for high albedo values. The relative RMSD is here calculated over the range of the measured data, while relative MedAE, MBE, MAE and STD are calculated over the mean. As RMSD score is very sensitive to outliers, it is

difficult to compare different data sets that do not have the same profile. Thus, we will mainly focus on MedAE, MBE and MAE scores to evaluate the differences between data sets. Med3 score will be used to assess the precision of each satellite product by calculating the absolute value of the difference between the center value and the corresponding linear interpolation between the two other values, for each triplet of consecutive values. The median of all these values is an indicator of the intra-annual precision of satellite albedo products (Sánchez-Zapero et al., 2020).

When we evaluate ETAL-R against ground stations measurements (or the MODIS product in the absence of these data), MedAE scores are compared to the following accuracy requirements (Table 4) from the Product Requirements Document (PRD) established in the framework of the LSA-SAF project. We consider that we meet the requirements when median values are below optimal or threshold requirements.

Validation strategy

Following the recommendations of CEOS (Wang et al., 2019), we evaluate ETAL-R based on inter-comparison with several data sets. In this study we use ETAL data from the NRT processing chain to check consistency at global scale and analyze stability for pseudo-invariant sites, as well as surface albedo from two different reference data sets for quality assessment, MODIS (Section 2.2.2) and *in situ* observations (Section 2.3). NRT ETAL, which was extensively validated against MODIS collection 6 surface albedo by Lellouch et al. (2020), is used to check consistency between ETAL-R and NRT ETAL, since the two products are expected to be combinable for forming long time series. The pixel-by-pixel analysis between NRT ETAL and MODIS done in that study showed low average MBE values of 5.8% and 0.001 for albedo values above and below 0.15, respectively. By comparing ETAL-R to NRT-generated ETAL, we aim to show the degree of agreement between the two data sets and the main differences coming from the different input data that were used to generate them.

Validation of ETAL-R goes through four major parts, based on the recommended quantities and practices shown in bold in Table 3:

- (1) **Consistency between ETAL-R and NRT-generated ETAL:** In Section 4.1, the consistency between the two satellite products is studied for the full globe and the 2015–2020 common period. Pixel-to-pixel comparison is used to assess ETAL-R against NRT ETAL on the same grid. A more in-depth comparison is made to understand the influence of seasons and latitudes. To this end, time series are generated for three regions defined according to latitude and using the tropics of Cancer (23.3°N) and Capricorn (23.3°S) as boundaries. Scores are also calculated for each northern hemisphere season and averaged over the full period to illustrate the seasonal variations.
- (2) **ETAL-R completeness and stability:** The product completeness and stability of ETAL-R is evaluated in Section 4.2. First, we generated (i) a map of the percentage of

missing data averaged over the year 2020 and (ii) a time series of the percentage of missing data averaged over the globe for each date. The temporal stability of ETAL-R is then investigated since 2007, as it is a good indication of the reliability of an albedo data set (Wang et al., 2019). The albedo stability of the ETAL-R product is evaluated for pseudo-invariant sites that are expected to present small changes in albedo over time.

- (3) **Local comparison against *in situ* reference data:** We consider specific regions of the globe with various types of land cover, to compare ETAL-R to reference albedo data. In Section 4.3, we focus on sites with available *in situ* measurements from ground stations. The *in situ* data are considered as reference for the accuracy and uncertainty assessment, and MODIS as well as NRT-generated ETAL are added for comparison to obtain the most complete analysis of ETAL-R. Ground stations are compared to ETAL-R data extracted from the closest

Table 5. Time period of the different albedo data sets used in this study.

Product	Available Time Period
ETAL-R	2007/01/25–2020/12/31
NRT-generated ETAL	2015/01/25–2020/12/31
MODIS	2017/01/01–2020/12/31
Stations GOB/MMS/PAY/CUMB/TATE	2017/01/01–2020/12/31
Station TBL	2017/01/01–2020/12/24

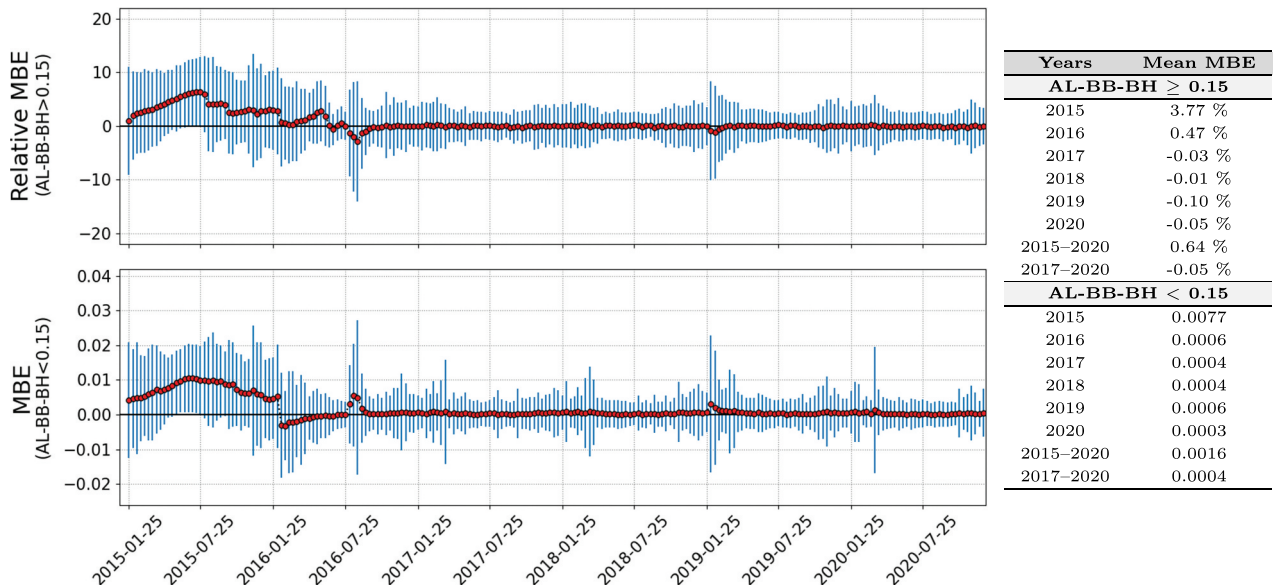


Figure 5. Time series of MBE (red points) and STD (blue vertical lines) for ETAL-R and NRT-generated ETAL, averaged for the full globe, for $AL-BB-BH \geq 0.15$ (top) and < 0.15 (bottom).

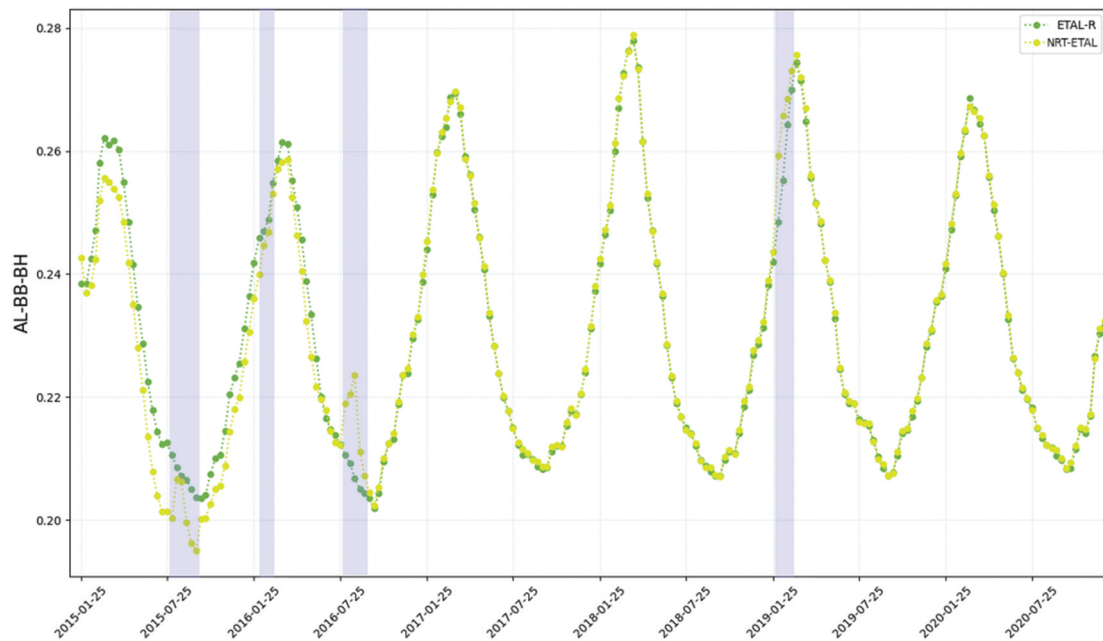


Figure 6. Time series of ETAL-R and NRT-generated ETAL AL-BB-BH averaged over the full globe with periods impacted by input data anomalies (blue areas).

pixel to the observation point, along with the closest MODIS pixel. The composite window used to compare each product is described in [section 2.3](#). These sites are also used to perform the precision evaluation of each satellite product.

- (4) **Local comparison with MODIS as reference:** In [Section 4.4](#), we extend the local analysis to several 10×10 pixels regions corresponding to additional cover types. At these locations, we compare against MODIS (MCD43D61 v006) for the time interval 2017-2020 (Metop-B) in order to expand the assessment of uncertainty and accuracy of ETAL-R.

To be accurate and representative of seasonal variations, validation is done over a sufficiently long time period from 2015 to 2020. Some time is also necessary for the ETAL products to converge to accurate estimates of surface albedo, due to the recursive nature of the Kalman filter. In this context, the comparison between ETAL-R and NRT-generated ETAL is made for the entire globe, for the time period of overlapping coverage from 1 January 2015 to 31 December 2020. The period from 1 January 2021 to 30 June 2021 was not available for ETAL-R at the time when the experiments were made and, therefore, was not included in the validation. The time period of each data set used in this study is detailed in [Table 5](#).

Results and discussion

Consistency between ETAL-R and NRT-generated ETAL

ETAL-R AL-BB-BH and AL-BB-DH surface albedo were compared against the corresponding NRT-generated ETAL data over the full globe. Differences between the two ETAL data sets were calculated for each pixel of the globe and each date of the full period for which these two products are available.

ETAL-R and NRT-generated ETAL AL-BB-BH biases were averaged over the full globe to produce MBE time series ([Figure 5](#)). For each date, pixels are separated in two groups, depending if the ETAL albedo value is above (top of the figure) or below (bottom of the figure) the 0.15 threshold. This threshold separates dark (below) from bright (above) surfaces. When looking at [Figure 5](#), we see the convergence of ETAL-R and NRT-generated ETAL, as the MBE score is close to zero from 2017 onward. Absolute scores do not go beyond 0.1% and 0.0006 for albedo values above and below 0.15, respectively. Larger biases observed before 2017 are due to a less accurate surface albedo from NRT-generated ETAL, which is still in the convergence phase. This is caused by the recursive retrieval method based on Kalman filtering.

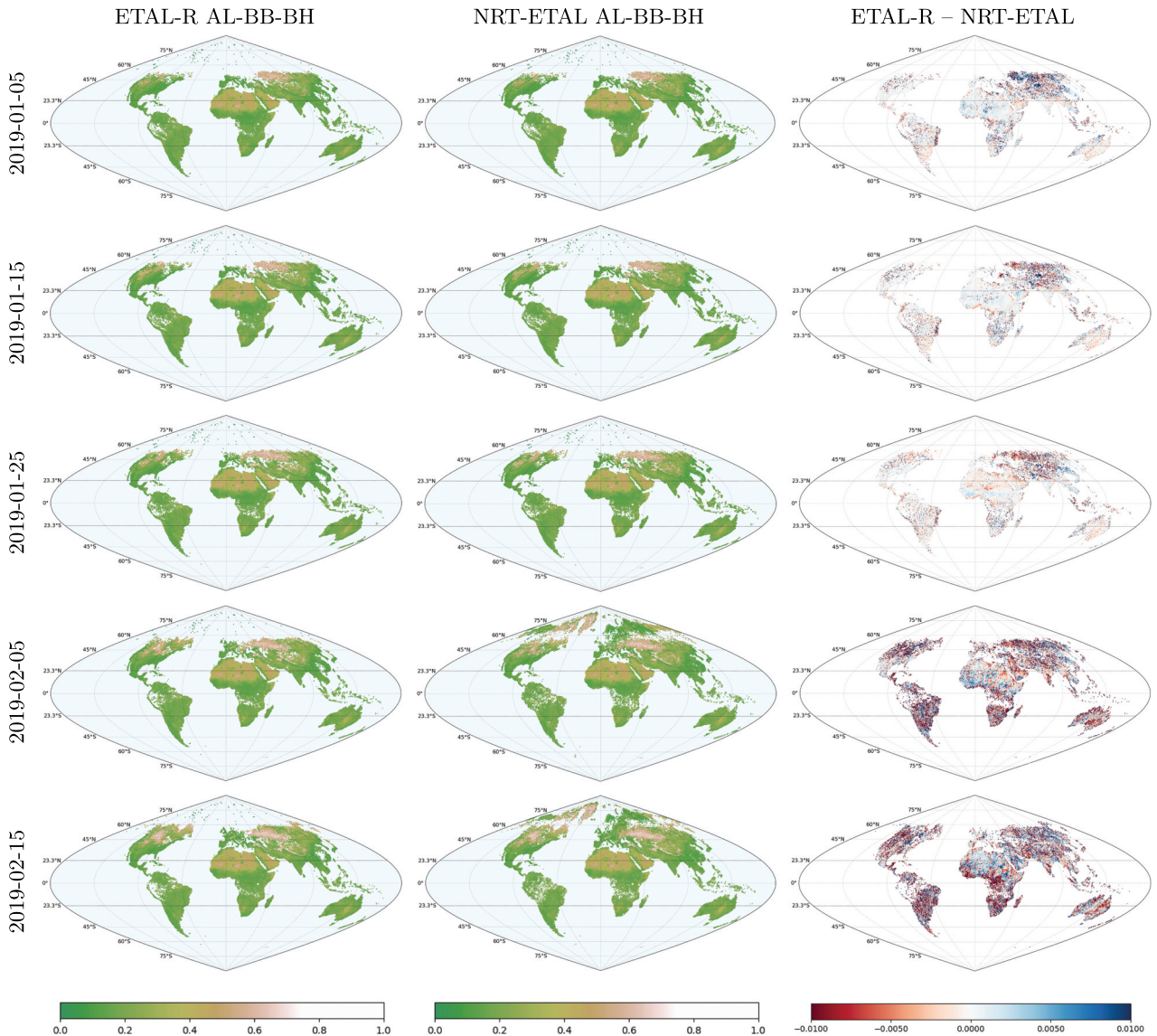


Figure 7. ETAL-R AL-BB-BH, NRT-generated ETAL AL-BB-BH and the difference between them.

Figure 5 highlights the convergence from 2017 but also draws attention to some occasional phenomena. First, we notice a jump in February 2016, particularly for albedo values below 0.15, then negative and positive peaks occur in August 2016, respectively, for albedo values above and below 0.15. After that, scores quickly converge towards 0, with a new small peak in February 2019. To understand better the origins of these anomalies, ETAL-R and NRT-generated ETAL AL-BB-BH bias averaged over the full globe is shown by Figure 6. Light blue areas emphasize the different anomalies, mentioned previously. For these periods, ETAL-R annual variations are smoother than those in NRT-generated ETAL. For example, NRT-ETAL presents abrupt changes in August 2015 and 2016, likely due to the use of corrupted ancillary input data, but also in February 2016 and 2019, when NRT-ETAL changes are smaller.

Since differences between ETAL-R and NRT-generated ETAL before 2017 can be affected by the period of convergence of the latter product, we therefore focus on the February 2019 anomaly. Figure 7 displays albedo maps of ETAL-R and NRT-generated ETAL, along with difference maps for four consecutive dates going from 15 January 2019 to 15 February 2019. The albedo maps do not show significant differences between the two data sets at first sight, as they are minor compared to the albedo magnitude. The sequence of maps showing the difference between ETAL-R and NRT-generated ETAL (Figure 7, 3rd column) reveals a certain continuity and stability until a sudden change happens on 5 February 2019 certainly related to the use of corrupted input data by the NRT ETAL chain. The first two dates, on the other hand, indicate very strong agreement between ETAL-R and NRT-generated ETAL, except over Asia. The generally very high global agreement between the two

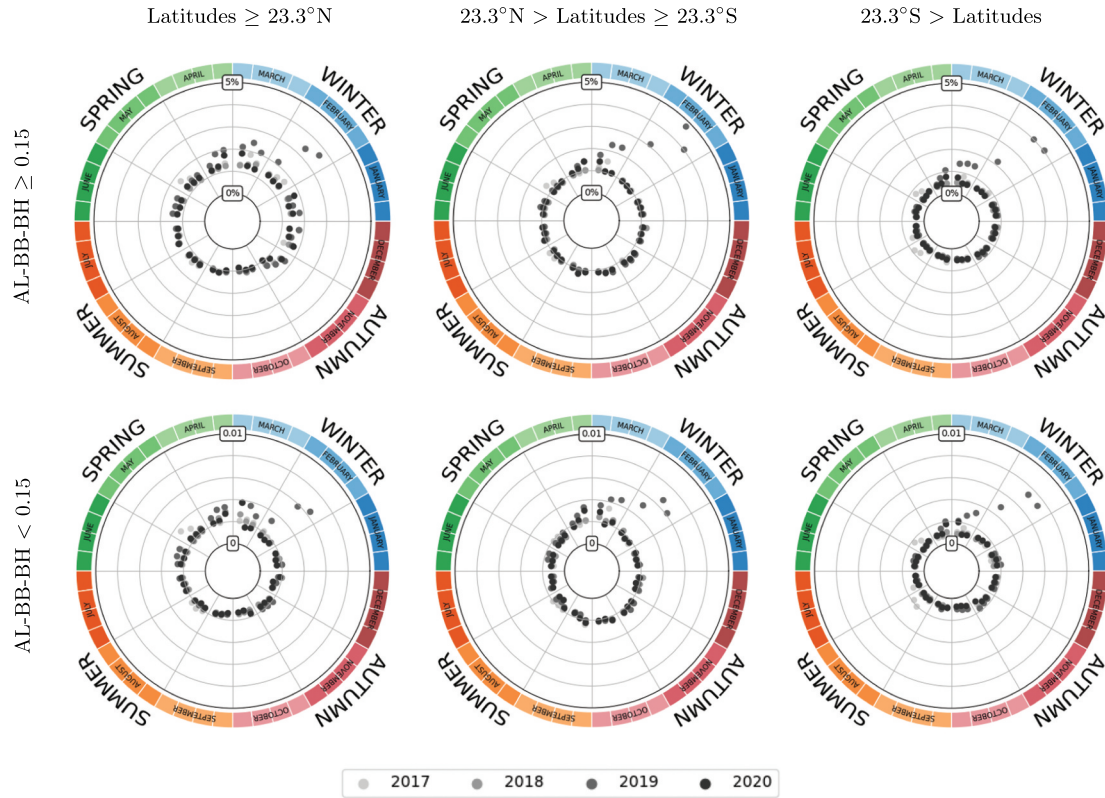


Figure 8. MAE score depending on latitudes, for AL-BB-BH ≥ 0.15 and < 0.15 . The seasons correspond to the Northern Hemisphere. This figure was made using scripts from Rougier (2021).

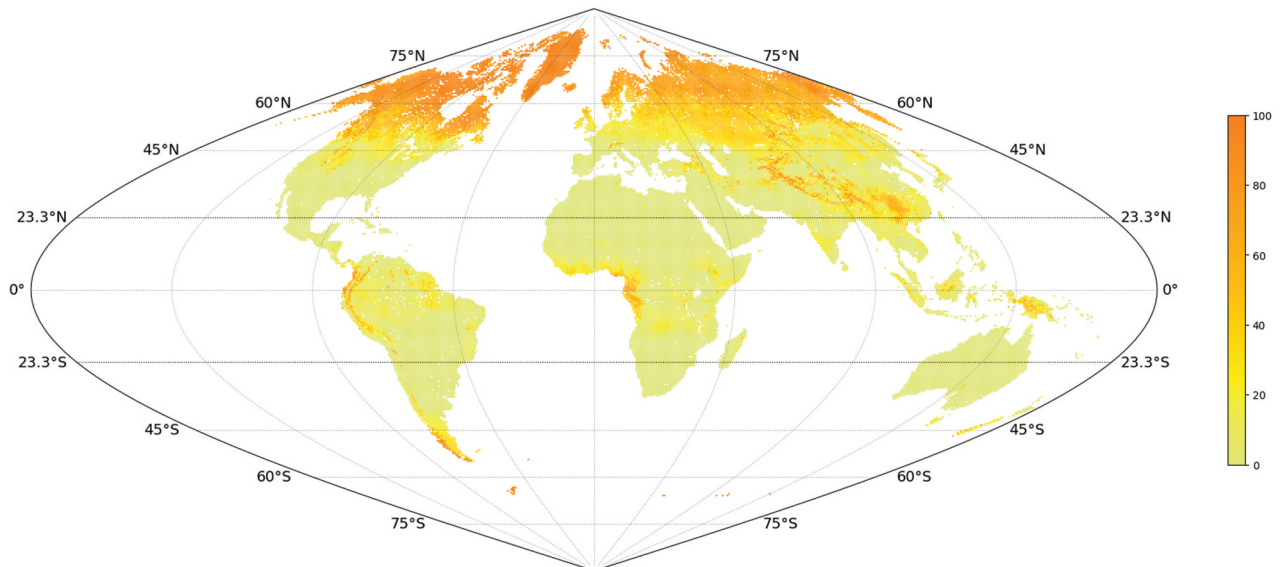


Figure 9. Percentage of missing data for ETAL-R AL-BB-BH averaged over 2020.

data sets (see also Figures 5 and 6) implies that there is little impact from switching from atmospheric forecasts to ERA-5 reanalyses. However, it is worth noting that the change of atmospheric inputs may be the cause of regional small (mostly < 0.01) differences such as those seen in Asia.

Based on the observed anomalies and the convergence of ETAL-R and NRT-generated ETAL from 2017 onwards, only the period from 2017 to 2020 will be used to further comparison of the two data sets.

To better understand the differences between ETAL-R and NRT-generated ETAL, MAE was calculated depending on latitudes and seasons. Figure 8 represents MAE scores for the 2017–2020 period, depending on latitudes and seasons, and highlights the convergence of the two products from 2017 onward. For each geographical zone, the evolution of the MBE is very similar. MAE scores are between 0.3% and 2.0% for albedo values above 0.15 and around 0.002 for albedo values below 0.15, with the exception



Figure 10. Percentage of missing data for ETAL-R and NRT ETAL AL-BB-BH averaged over the globe for 2020.

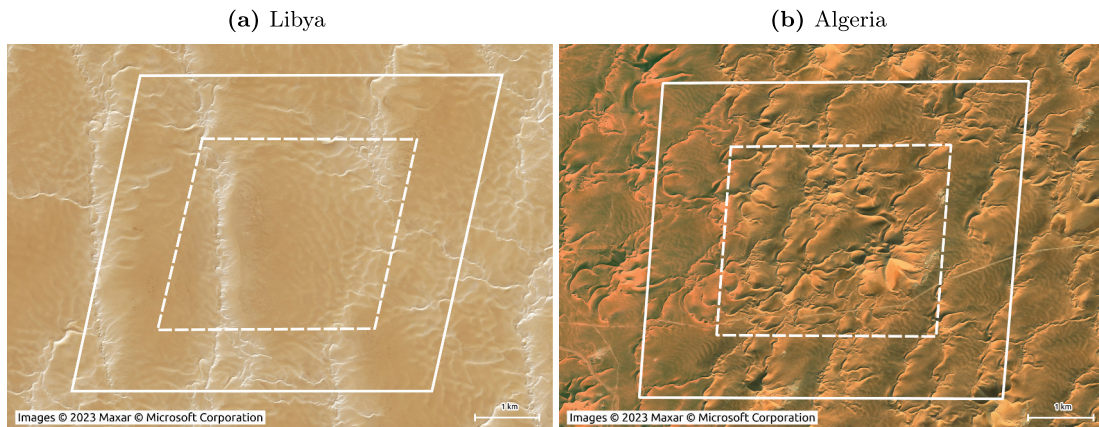


Figure 11. Approximate footprints of both 3×3 and 5×5 ETAL data sets for each studied areas, respectively shown in dashed and solid white line.

of February and March 2019, where the MAE score increases for both albedo values above and below 0.15 due to the anomaly described above. The MAE score is slightly higher in winter, over a longer period for the higher latitudes due to the presence of snow in the Northern Hemisphere. The seasonal variations of AL-BB-DH (Figure A.4) follow the same pattern, with slightly higher (lower) values for northern (between and southern) latitudes.

Completeness and stability of ETAL-R

Completeness is quantified by “1 - proportion of missing data” over the entire globe at any given time. In our case, it was evaluated for the year 2020 as we only expect seasonal variations. Figure 9 evaluates for ETAL-R the distribution in space while Figure 10 the distribution in time of missing data for both ETAL-R and NRT ETAL. Both figures show that ETAL-R is not well represented for latitudes above 45° and around

the equator, especially during winter in the northern hemisphere with gaps close to 35% across the globe (the northern hemisphere has significantly more land pixels at 45° and above). This may be due to the presence of clouds or the effect of shorter days in winter. The percentage of missing data is lowest in September with a value close to 10%. ETAL-R and NRT ETAL are very similar on this aspect, with a slight difference between March and April. AL-BB-DH results are presented in Appendix A and are very similar to the AL-BB-BH results.

As described in Wang et al. (2019), the evaluation of the stability requires to study large areas, of 3×3 and 5×5 pixels around the target location, plot the time series of mean using STD as uncertainty and estimate the regression slope to evaluate the trend. It is recommended to select bright desert areas with very low annual variations. The regions used to evaluate the temporal stability of the ETAL-R product cover then homogeneous areas over Libya (28.55°N , 23.39°E) and Algeria (30.32°N , 7.66°E)

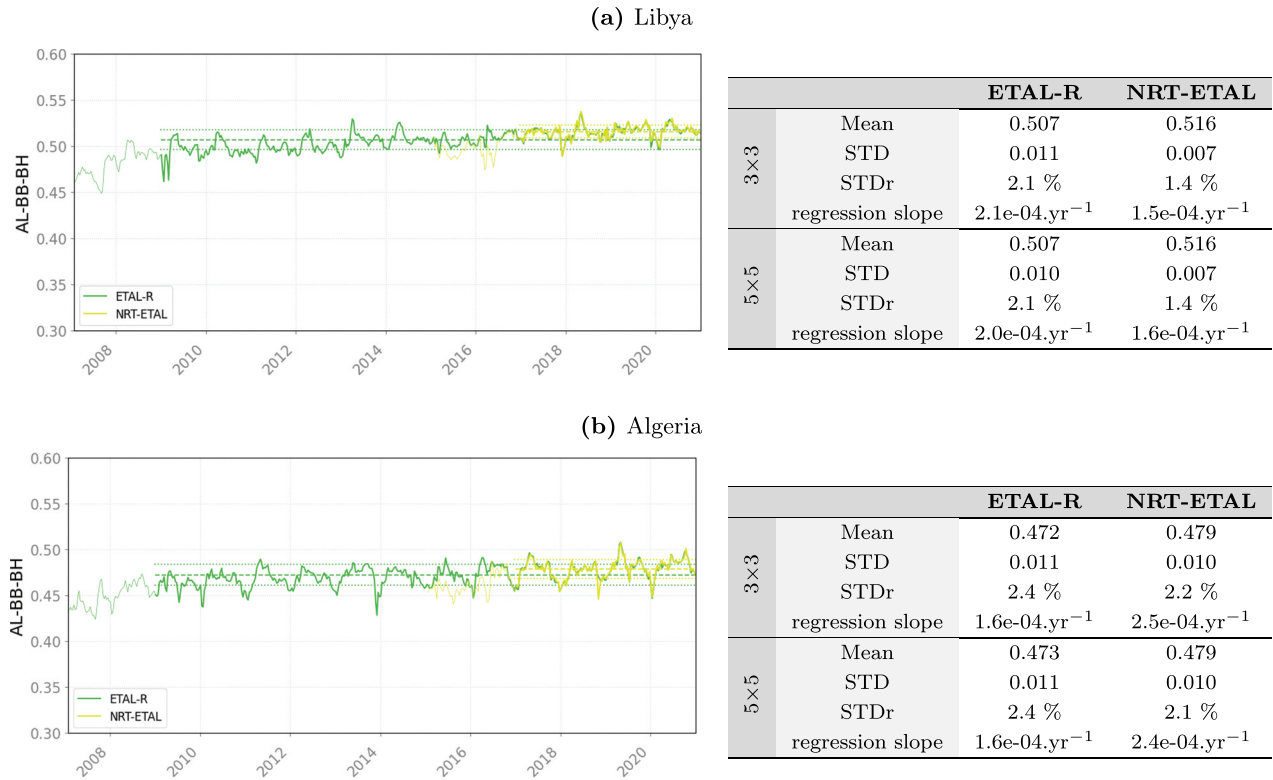


Figure 12. Time series of ETAL-R and near-real time generated ETAL AL-BB-BH surface albedo 3×3 pixels area with various scores for both 3×3 and 5×5 pixels area. Dashed lines represent the mean of the time series and dotted lines the temporal standard deviation. First two years are grayed out because they were not considered in the calculation of the scores due to the convergence phase of ETAL-R.

corresponding to desert areas (see Figure 11). Their position is indicated by black crosses in Figure 3. These areas have been chosen because they are pseudo-invariant sites identified by the United States Geological Survey (USGS, 2020) for the calibration of space-based optical imaging sensors because of their high radiometric stability and size. Figure 12 displays AL-BB-BH surface albedo time series from 25 January 2007 to 31 December 2020, for 3×3 pixels over these regions with scores for both 3×3 pixels and 5×5 pixels areas. Results for AL-BB-DH are presented in Appendix A.

For each region, we calculate the mean, temporal standard deviation, relative standard deviation, and regression slope of the time series. Due to the Kalman filter used by the albedo algorithm, the ETAL data take some time to converge. We estimated, from Figure 5, this period to be of one and a half years for the NRT-generated ETAL. In order to be representative, the first two years of the data were removed from the calculation for both ETAL data sets. Figure 12 confirms the stability of ETAL-R by showing a very small and therefore not significant slope for both satellite products and areas. We, however, note the generally positiveness of this slope,

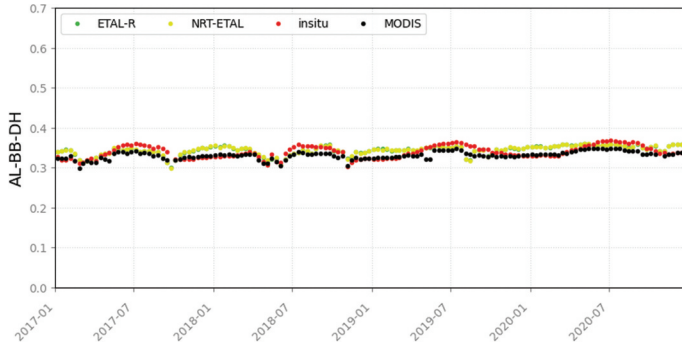
which may be related to a drift in the AVHRR data calibration during the satellites lifetime. After convergence, ETAL-R and NRT-generated ETAL have the same variations and regularity. The STDr is between 1.4% and 2.3% for both ETAL-R and NRT-generated ETAL.

Local comparison against in situ reference data

The *in situ* data obtained from the stations GOB, MMS, TBL, CUMB, PAY, and TATE (see Section 2.3) are used as reference for the calculation of the following scores. Scores are given in relative or absolute values depending on the predominant albedo mode (either greater or lower than 0.15) for simplicity.

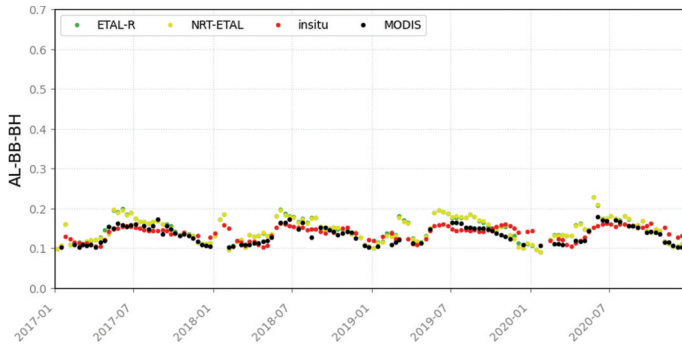
According to Figures 13 and 14 showing the time series for all ground stations, ETAL-R gets almost identical scores to NRT-generated ETAL for all stations. Scores of RMSD are similar to MODIS for PAY and CUMB, better than MODIS for TBL and TATE and worse than MODIS for GOB and MMS. MedAE, MAE and MBE appear slightly better for MODIS in general but it should be taken into account that MODIS data seem to be subject to further filtering, taking into

(a) GOB



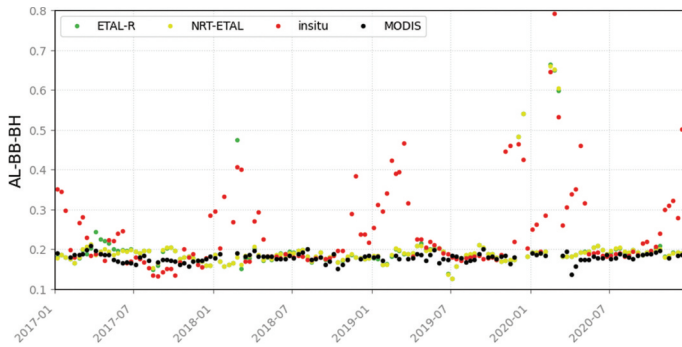
	ETAL-R	NRT-ETAL	MODIS
MedAE	3.6 %	3.6 %	2.1 %
MBE	1.7 %	1.7 %	-2.3 %
MAE	3.9 %	3.9 %	2.8 %
RMSD	28.8 %	29.0 %	24.9 %
N	140	140	139
R	0.45	0.45	0.81
Med3	0.0018	0.0019	0.0015

(b) MMS



	ETAL-R	NRT-ETAL	MODIS
MedAE	0.017	0.016	0.009
MBE	0.012	0.011	-0.002
MAE	0.020	0.020	0.011
RMSD	0.018	0.018	0.009
N	118	118	88
R	0.66	0.66	0.76
Med3	0.0058	0.0056	0.0020

(c) TBL



	ETAL-R	NRT-ETAL	MODIS
MedAE	12.6 %	12.1 %	9.5 %
MBE	-11.7 %	-12.5 %	-13.4 %
MAE	19.3 %	19.4 %	16.4 %
RMSD	14.3 %	14.6 %	90.0 %
N	138	138	120
R	0.63	0.62	-0.01
Med3	0.0047	0.0048	0.0040

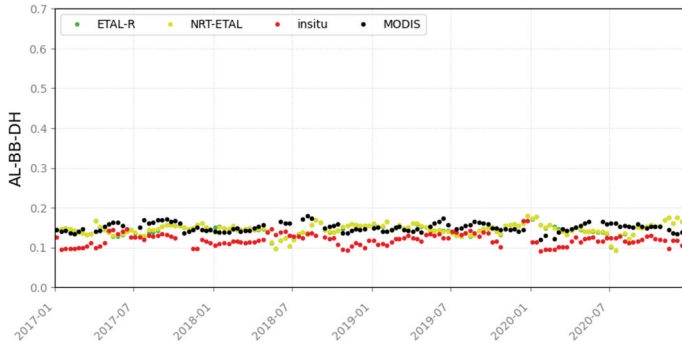
Figure 13. Time series of ETAL-R, NRT-generated ETAL, and MODIS compared to ground observations with homogeneous satellite footprint. Errors for stations/locations with albedo > 0.15 are given in percent, while absolute errors are used for those with albedo < 0.15 (see Section 3.2).

account the lower number of available points for all stations. The scores are better for the stations with the most visually homogeneous satellite footprint, i.e. MMS, GOB and TBL, than for the three others.

For MMS, ETAL-R and NRT-generated ETAL slightly overestimate the albedo in summer but the *in situ* seasonal trend is well captured, while for GOB, ETAL-R and NRT-generated ETAL are closer to *in situ* data in summer whereas MODIS is closer in winter. Too low values of MODIS albedo for GOB with respect to ground measurements and the PROBA-V satellite product were also observed by Sánchez-Zapero et al. (2020),

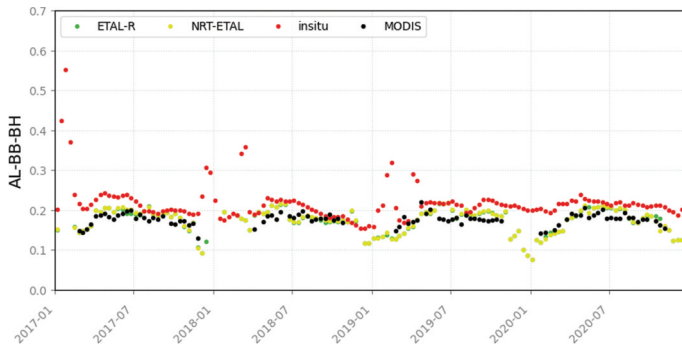
who interpreted this as a bias in the MODIS product. For CUMB, PAY, TATE and TBL, the *in situ* annual trend is globally respected by the three satellite products. However, the snow episodes are not captured by MODIS while the two ETAL data sets occasionally succeed. For TBL, ETAL-R and NRT-generated ETAL indeed manage to capture a few snow events, while it is not the case for PAY, where albedo values seem to decrease too much with respect to *in situ* data. We note an approximate 0.07 underestimation for each satellite product for TATE, and although each satellite seems to capture annual variations for CUMB, they tend to

(a) CUMB



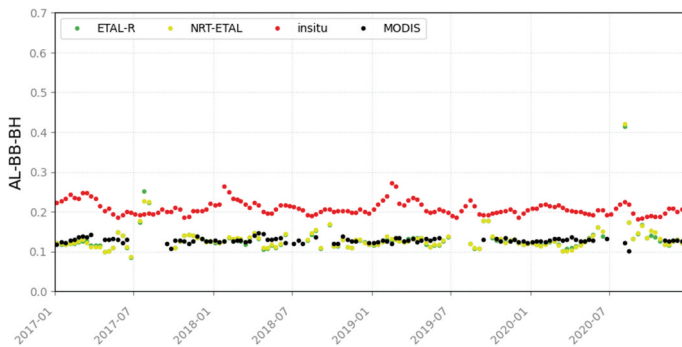
	ETAL-R	NRT-ETAL	MODIS
MedAE	0.030	0.029	0.033
MBE	0.026	0.026	0.033
MAE	0.030	0.030	0.033
RMSD	0.027	0.027	0.025
N	134	134	114
R	-0.37	-0.35	0.71
Med3	0.0033	0.0032	0.0030

(b) PAY



	ETAL-R	NRT-ETAL	MODIS
MedAE	15.1 %	13.8 %	17.4 %
MBE	-18.0 %	-17.4 %	-16.3 %
MAE	18.6 %	18.1 %	16.6 %
RMSD	20.8 %	19.8 %	19.6 %
N	135	134	96
R	0.14	0.19	0.33
Med3	0.0051	0.0051	0.055

(c) TATE



	ETAL-R	NRT-ETAL	MODIS
MedAE	41.7 %	41.5 %	38.7 %
MBE	-37.1 %	-36.9 %	-39.0 %
MAE	39.2 %	38.7 %	39.0 %
RMSD	20.2 %	19.8 %	132.9 %
N	125	125	102
R	-0.04	-0.05	0.05
Med3	0.0036	0.0038	0.0025

Figure 14. Time series of ETAL-R, NRT-generated ETAL and MODIS compared to ground observations with heterogeneous satellite footprint. Errors for stations/locations with albedo > 0.15 are given in percent, while absolute errors are used for those with albedo < 0.15 (see Section 3.2).

Table 6. List of areas with the center of ETAL-R, NRT-generated ETAL and MODIS 10×10 pixels position. Surface types were determined by using MODIS-IGBP land cover (500 m) layer from Boston University and NASA LP DAAC (Friedl & Sulla-Menashe, 2019).

Country	ETAL-R and NRT-ETAL		MODIS		Distance between center points	Surface type
	Lat	Lon	Lat	Lon		
Australia	-16.5950	127.1825	-16.6000	127.1917	691 m	Open Shrublands
Democratic Republic of the Congo	0.3150	21.5253	0.3167	21.5333	847 m	Evergreen broadleaf
Kazakhstan	48.4750	49.5892	48.4750	49.5917	301 m	Grassland
Mozambique	-20.4450	33.5803	-20.4500	33.5833	474 m	Savannas

overestimate albedo values, with a much better correlation for MODIS. Please note the absence of data from MODIS in winter for most stations, which may point to high cloudiness or a generally low representativeness of the ground station footprint at this time of the year.

In conclusion, ETAL-R meets the threshold requirements of 20% and 0.03 for all stations except TATE as expected due the lack of spatial representativeness. Target and optimal requirements are also met for MMS and GOB, respectively (see Table 4). It is

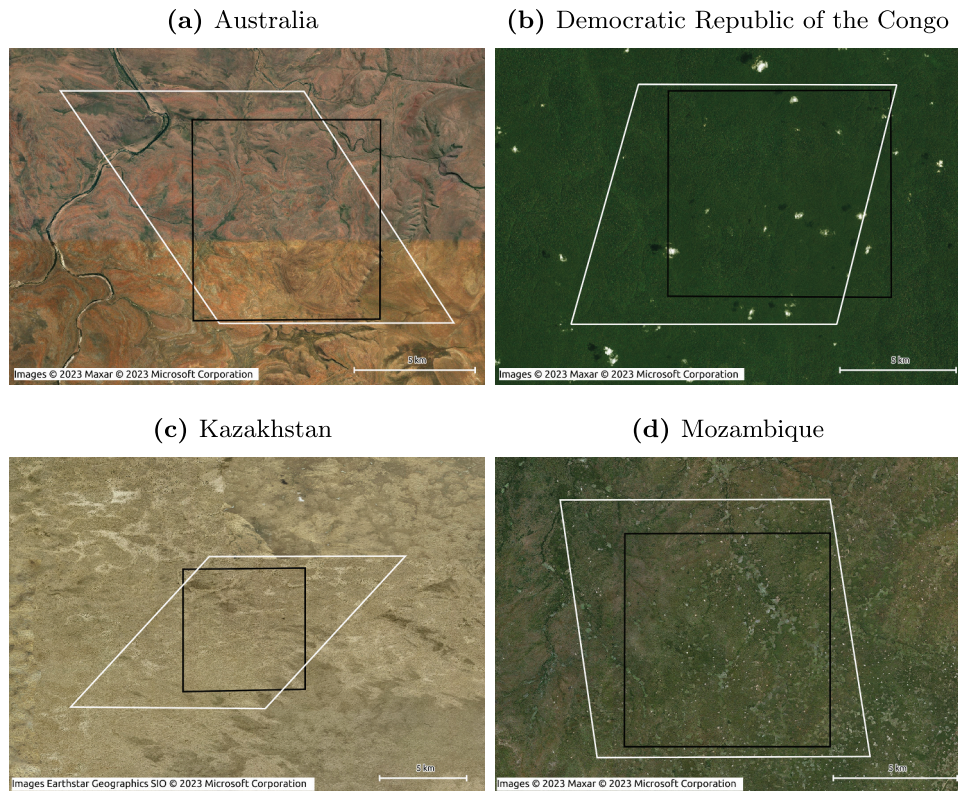


Figure 15. Approximate footprints for studied areas of both ETAL data sets (white) and MODIS (black).

worth noting that stations with homogeneous satellite footprint also achieved better scores than those with heterogeneous satellite footprint.

The precision of each satellite product is here calculated over all the validation sites between 2017 and 2020 with median of 3-point difference (Med3). Scores are shown in the tables of [Figures 13 and 14](#). For most stations, ETAL-R, NRT-ETAL, and MODIS present similar values. MMS and TATE are the exception, with higher values for ETAL-R and NRT-ETAL.

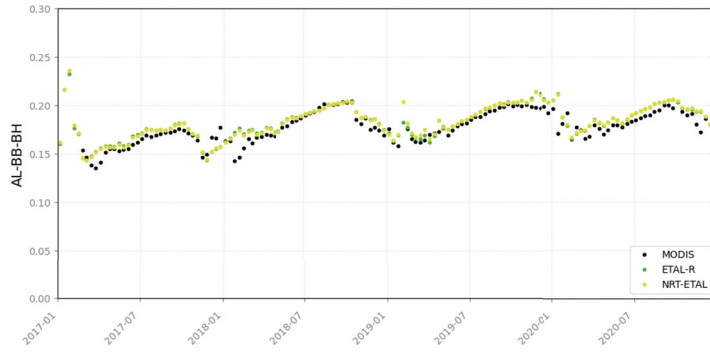
Local comparison with MODIS as reference

Four additional local areas (see [Table 6](#)) were selected according to their diversity of land cover types to complement the previous comparison to ground stations. Their position is indicated by red circles in [Figure 3](#). The sites correspond to homogeneous areas of open shrublands, evergreen broadleaf forest, grassland and savannas ([Figure 15](#)). Here, MODIS is taken as the reference data in the absence of *in situ* measurements. For this comparison we use relatively large and homogeneous areas of 10×10 pixels.

[Figure 16](#) shows very similar scores between ETAL-R and NRT-generated ETAL. Again, results are given for the predominant albedo mode only

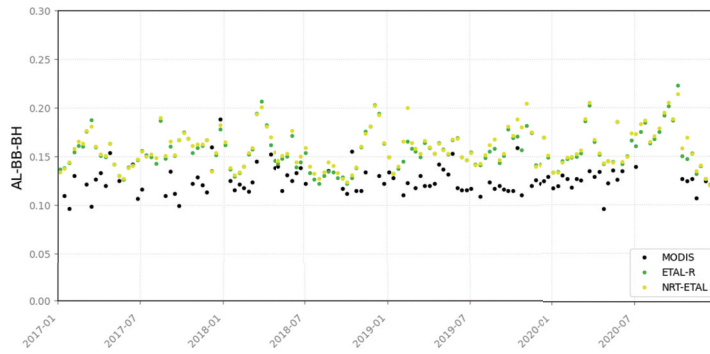
(either greater or lower than 0.15) for simplicity. Australia presents satisfactory MedAE scores of 2.8% and 2.9% for ETAL-R and NRT-generated ETAL, below the 5% required by the optimal requirements. MODIS albedo variability is indeed well captured, with R values of 0.90 and 0.91 for ETAL-R and NRT-generated ETAL, respectively. The results for the Democratic Republic of Congo allow ETAL-R to meet the threshold requirements, with MedAE scores of 0.030. While all satellite products provide stable albedo values, with no regular seasonal variation, ETAL-R and NRT-generated ETAL appear to be occasionally affected by greater variability which may be related to residual cloud contamination. MedAE scores for Kazakhstan allow ETAL-R and NRT-generated ETAL to meet the target requirements, with respectively MedAE of 8.1% and 8.0%. For this station, the variability of MODIS albedo is very well captured, along with the snow episodes, resulting in a correlation R equal to 0.97 for both ETAL-R and NRT-generated ETAL. Regarding Mozambique, all satellite products follow similar seasonal variations, even though the two ETAL data sets present greater albedo peaks than MODIS. MedAE scores are 0.017 and 0.018 for both satellite products, which allows them to meet the threshold requirements.

(a) Australia



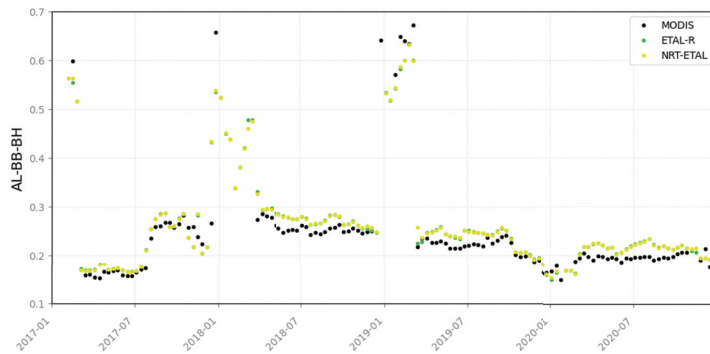
	ETAL-R	NRT-ETAL
MedAE	2.8 %	2.9 %
MBE	2.5 %	2.5 %
MAE	3.4 %	3.3 %
RMSD	11.4 %	11.3 %
N	128	128
R	0.90	0.91

(b) Democratic Republic of the Congo



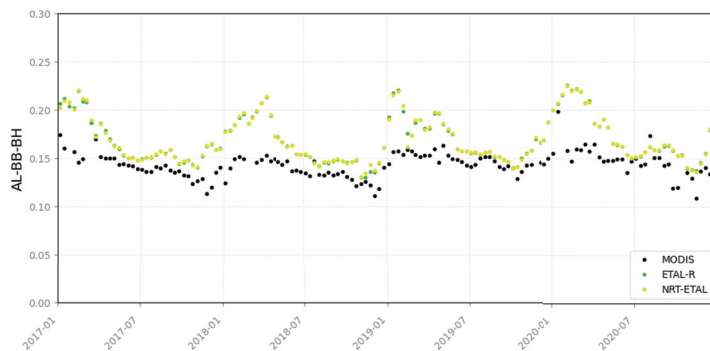
	ETAL-R	NRT-ETAL
MedAE	0.030	0.032
MBE	0.030	0.032
MAE	0.030	0.032
RMSD	0.029	0.031
N	95	95
R	0.12	0.13

(c) Kazakhstan



	ETAL-R	NRT-ETAL
MedAE	8.1 %	8.0 %
MBE	6.5 %	6.6 %
MAE	8.9 %	8.8 %
RMSD	6.1 %	6.1 %
N	119	119
R	0.97	0.97

(d) Mozambique



	ETAL-R	NRT-ETAL
MedAE	0.017	0.018
MBE	0.024	0.024
MAE	0.024	0.024
RMSD	0.029	0.029
N	137	137
R	0.65	0.64

Figure 16. Time series of ETAL-R and NRT-generated ETAL AL-BB-BH compared to MODIS with statistics scores. Errors for stations/locations with albedo > 0.15 are given in percent, while absolute errors are used for those with albedo < 0.15 (see Section 3.2).

The results reported here were found to be generally better for BSA (data variable AL-BB-DH), with MedAE scores allowing to meet the target requirements instead of the threshold ones for Mozambique.

Product showcase: albedo variations in the Sahel region

In order to present the interest of ETAL-R, an illustrating case study was carried out on the Sahel region. Located in Africa, the Sahel is the belt that marks the transition between the Sahara in the north and the savannas in the south, from east to west of the continent.

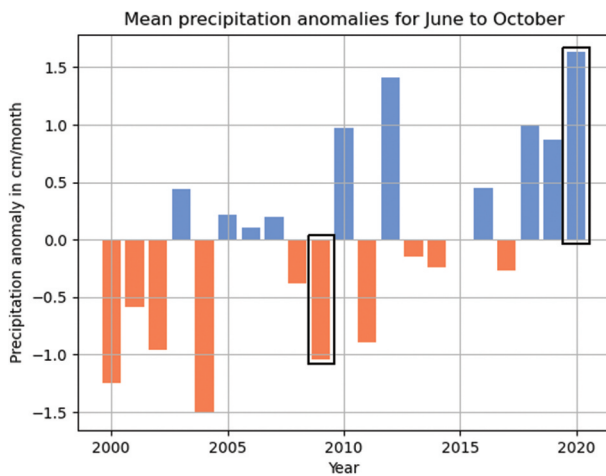


Figure 17. Mean precipitation anomalies (cm/month) for June to October in the region for latitudes from 12°N to 20°N and longitudes from 0°E to 20°E. Years 2009 and 2020 are framed in black.

Here, we follow the work from Govaerts and Lattanzio (2008) who studied the consequences on surface albedo of the extreme drought happened in the Sahel region in the 1970s and 1980s. By comparing the years 1984 and 2003 the authors showed that the deficit in precipitation caused an increase in albedo of 0.06 during these years, which they linked to the increased vegetation growth in the year with higher precipitation after the drought.

We conducted a similar comparison of the surface albedo between the years 2009 and 2020. Figure 17 shows higher precipitation (based on *GPM IMERG Final Precipitation L3 1 month 0.1° × 0.1° V06* from Huffman et al. (2019)) in 2020 than in 2009, over an area running from 0°E up to 20°E and from 12°N up to 20°N. The surface albedo bias between 2020 and 2009, averaged over August and September, is represented in Figure 18. We can see a blue band in the black box running from 5°W up to 30°E and from 12.5°N up to 16.5°N, meaning that the surface albedo in 2020 was lower than in 2009. Precipitation in 2020 being significantly higher than that in 2009, we assume that the mechanism for the change in albedo is the same as the one found by Govaerts and Lattanzio (2008), i.e. an increase in vegetation growth in years of higher precipitation. Additionally, the lower reflectance of wet soil as compared to dry soil may contribute to the observed change in surface albedo as well.

Figure 19 shows a significant decrease in albedo in 2020 of around 0.08, compared to 2009 with a drop of around 0.04. We can note that years with biggest drops in the albedo (2010, 2012, 2018 and 2020) are also the years with the higher precipitation anomalies between June and October (see Figure 17).

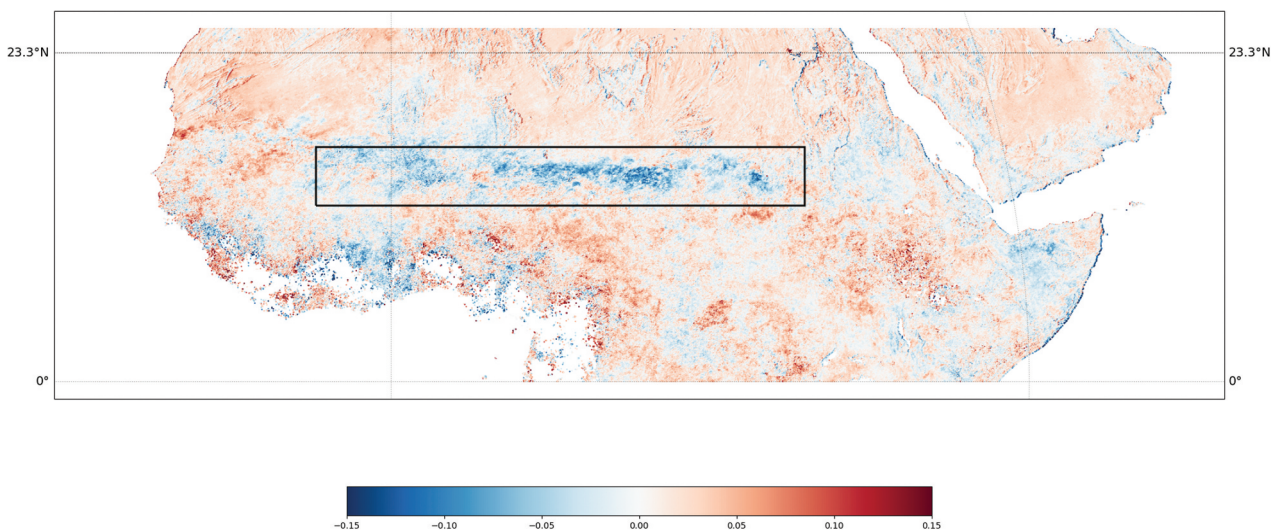


Figure 18. ETAL-R AL-BB-BH bias between 2020 and 2009, averaged over the months of August and September of each year over the Sahel region.

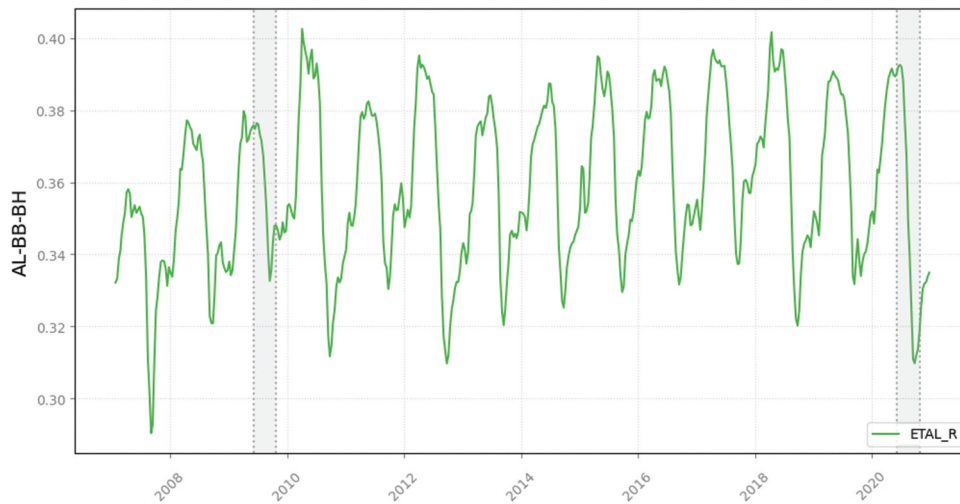


Figure 19. ETAL-R AL-BB-BH time series from 2007 to 2020, averaged over the region covered by latitudes from 12.5°N to 16.5°N and longitudes from 5°W to 30°E. The June–October 2009 and June–October 2020 periods are grayed out.

Conclusions

The back-processed ETAL-R data record complements the near-real time generated ETAL archive, covering a longer period of time and using more consistent reanalyzed input data including information on atmospheric constituents. ETAL-R aims to be more stable and homogeneous than the NRT-generated data while keeping the consistency between the two retrievals.

To assess the quality of ETAL-R, global and local comparisons were carried out for the period from January 2015 to December 2020. Scores of MBE for WSA (data variable AL-BB-BH) were found to be very satisfactory for with values of 0.64% (for albedo values above 0.15) and 0.0016 (for albedo values below 0.15) for the full period and globe. ETAL-R was found to be better in terms of stability and robustness with respect to NRT-generated ETAL, which was found to be affected by a few errors due to occasional missing or bad input data. Furthermore, the NRT-generated ETAL was found to be slightly different with respect to ETAL-R in 2015–2016 as it was in the pre-convergence period of the Kalman filter included in the retrieval algorithm. By looking further into the differences for the 2017–2020 post-convergence period, we can see a very high consistency between ETAL-R and NRT-generated ETAL. A latitude-based analysis showed that differences are generally low with MAE scores between 0.3% and 2.0% for albedo values above 0.15 and around 0.002 for albedo values below 0.15. The larger differences can be found in the Northern Hemisphere due to the presence of snow and ice with naturally higher albedo values. The observed consistency between the two datasets

is important because it allows users to combine the two datasets into long running time series which may be useful for many applications, for example the analysis of environmental changes over long time scales.

ETAL-R completeness was assessed over 2020, showing a lack of representativeness for high latitudes and the equator, especially during the northern hemisphere winter, probably due to snowy and cloudy episodes. Stability of ETAL-R was then demonstrated over the full period of availability of the product, with no spurious long-term trend observed from 2007 to 2020. Annual variations were found to be naturally more pronounced for 3×3 pixels forest regions than deserts, with STD_r of 15.2% for the first, and 1.8% and 3.8% for the latter.

When comparing ETAL-R with ground measurements, we noticed that the back-processed data product obtains similar scores to the NRT-generated ETAL. Both ETAL data sets were found to be comparable to MODIS data over the selected ground stations. In particular, ETAL-R was found to be closer to ground measurements than MODIS for stations CUMB, TBL and GOB but more different for stations TATE, MMS and PAY. Stations with homogeneous satellite footprint present the best MedAE scores for each satellite. The comparison over additional 10×10-pixel regions allowed a broader consideration of land covers. Overall, ETAL-R was found to be relatively close to MODIS and to follow the same annual variations. For savannas and forests in Central Africa, however, ETAL-R and NRT-generated ETAL were observed to overestimate the albedo measured by MODIS. This discrepancy could be caused by different reasons including distinct aerosol correction (Moparthy et al., 2019), residual cloud contamination

or other algorithmic differences between ETAL and MODIS. Finally, threshold requirements (MedAE of 20% and 0.03) were found to be met for all stations with homogeneous satellite footprint (with respect to *in situ* data) and local regions (with respect to MODIS data), with some cases meeting the more demanding target (MedAE of 10% and 0.015) and optimal (MedAE of 5% and 0.0075) requirements. Assessment of BSA (data variable AL-BB-DH) obtained similar or better results for all experiments overall. When comparing ETAL-R and NRT-ETAL with MODIS, it is important to note that the satellites do not have exactly the same coverage or sliding temporal window, which can have an impact on their differences.

We also present an illustrating subset of the data from the Sahel region in Africa to showcase a possible application of ETAL-R, highlighting the correlation between surface albedo evolution and episodes of drought or intense rainfall. Apart from direct applications such as the one presented, ETAL-R and NRT-ETAL products are of importance for the processing of downstream LSA SAF vegetation products (leaf area index, fraction of absorbed photosynthetically active radiation, fractional vegetation cover).

The results that we present here show that ETAL-R can be considered a reliable global surface albedo record for the time interval from 2007 to 2021 and that it meets the LSA SAF product requirements. ETAL-R and the current archive of ETAL (the original NRT processing) form a fairly consistent set and can therefore be connected over the transition from 2021 to 2022. At the same time, the ETAL-R back-processing fixes certain shortcomings of the NRT ETAL archive that stem from the near-real time nature of the original processing, such as problems with ancillary inputs. ETAL-R will replace the current, downloadable ETAL archive for 2015 to 2021 (and add the years 2007 to 2015) once an internal review process is complete. The update of the ETAL archive by the incorporation of ETAL-R will be announced by the LSA SAF (<http://lsa-saf.eumetsat.int/>). New versions of ETAL-R may be generated in the future as part of the continuous development carried out in the EUMETSAT SAFs. Future EPS albedo data records may be upgraded by including an improved radiometric calibration of the different AVHRR sensors along the lifetime of the different satellites (e.g. Metop-A, Metop-B), provided that this information is made available by EUMETSAT.

Acknowledgments

This study has been undertaken using data from GBOV “Ground Based Observation for Validation” (<https://land.copernicus.eu/global/gbov>) founded by European Commission Joint Research Centre FWC932059, part of the Global Component of the European Union’s Copernicus Land Monitoring Service. GBOV products are

developed and managed by ACRI-ST with the support from University College London, University of Leicester, University of Southampton, University of Valencia and Informus GmbH. We thank John A. Augustine and the SURFRAD network for the measurements collected in the field and used to generate GBOV products. *In situ* data from the AmeriFlux network is used in this study (MMS; Novick and Phillips, 2022). Funding for the AmeriFlux data portal was provided by the U.S. Department of Energy Office of Science. And finally, data from BSRN through the PANGAEA data portal were used (Vogt, 2021; Vuilleumier, 2021). This work was done within the framework of the LSA SAF (<http://lsa-saf-eumetsat.int>) project, funded by EUMETSAT. Finally, Rémy Fransen is kindly acknowledged for his contribution to the early phase of this work.

Disclosure statement

No potential conflict of interest was reported by the author(s).

Funding

The work was supported by the European Organization for the Exploitation of Meteorological Satellites [LSA-SAF CDOP-4].

Data availability statement

The ETAL-R data that support the findings of this study will be soon openly available at <https://landsaf.ipma.pt/en/products/albedo/etal/>.

References

- Becerril-Piña, R., Díaz-Delgado, C., Mastachi-Loza, C. A., & González-Sosa, E. (2016). Integration of remote sensing techniques for monitoring desertification in Mexico. *Human & Ecological Risk Assessment*, 22(6), 1323–1340. <https://doi.org/10.1080/10807039.2016.1169914>
- Carrer, D., Moparthy, S., Lellouch, G., Ceamanos, X., Pinault, F., Freitas, S., & Trigo, I. (2018). Land surface albedo derived on a Ten daily basis from meteosat second generation observations: The NRT and climate data record collections from the EUMETSAT LSA SAF. *Remote Sensing*, 10(8), 1262. <https://doi.org/10.3390/rs10081262>
- Cedilnik, J., Carrer, D., Mahfouf, J., & Roujean, J. (2012). Impact assessment of daily satellite-derived surface albedo in a limited-area NWP model. *Journal of Applied Meteorology and Climatology*, 51(10), 1835–1854. <https://doi.org/10.1175/JAMC-D-11-0163.1>
- Dirmeyer, P. A., & Shukla, J. (1994). Albedo as a modulator of climate response to tropical deforestation. *Journal of Geophysical Research-Atmospheres*, 99(10), 20863–20877. <https://doi.org/10.1029/94JD01311>
- Driemel, A., Augustine, J., Behrens, K., Colle, S., Cox, C., Cuevas-Agulló, E., Denn, F. M., Duprat, T., Fukuda, M., Grobe, H., Haeffelin, M., Hodges, G., Hyett, N., Ijima, O., Kallis, A., Knap, W., Kustov, V., Long, C. N. . . . König-Langlo, G. (2018). Baseline surface radiation network (BSRN): Structure and data description (1992–2017). *Earth System Science Data*, 10(3), 1491–1501. <https://doi.org/10.5194/essd-10-1491-2018>

- Friedl, M., & Sulla-Menashe, D. (2019). MCD12Q1 MODIS/Terra+qua Land Cover Type Yearly L3 Global 500m SIN Grid V006, NASA EOSDIS Land Processes DAAC.
- Geiger, B., Carrer, D., Franchisteguy, L., Roujean, J.-L., & Meurey, C. (2008). Land surface albedo derived on a daily basis from meteosat second generation observations. *IEEE Transactions on Geoscience & Remote Sensing*, 46(11), 3841–3856. <https://doi.org/10.1109/TGRS.2008.2001798>
- Govaerts, Y., & Lattanzio, A. (2008). Estimation of surface albedo increase during the eighties sahel drought from meteosat observations. *Global and Planetary Change*, 64(3–4), 139–145. <https://doi.org/10.1016/j.gloplacha.2008.04.004>
- Hersbach, H., Bell, B., Berrisford, P., Hirahara, S., Horányi, A., Muñoz-Sabater, J., Nicolas, J., Peubey, C., Radu, R., Schepers, D., Simmons, A., Soci, C., Abdalla, S., Abellan, X., Balsamo, G., Bechtold, P., Biavati, G., Bidlot, J. ... Villaume, S. (2021). The ERA5 global reanalysis. *Quarterly Journal of the Royal Meteorological Society*, 146(730), 1999–2049. <https://doi.org/10.1002/qj.3803>
- Huffman, G., Stocker, E., Bolvin, D., Nelkin, E., & Tan, J. (2019). GPM IMERG final precipitation L3 1 month 0.1°×0.1° v06, greenbelt, md. *Goddard Earth Sciences Data and Information Services Center (GES DISC)*. <https://doi.org/10.5067/GPM/IMERG/3B-MONTH/06>
- Juncu, D., Ceamanos, X., Trigo, I. F., Gomes, S., & Freitas, S. C. (2022). Upgrade of LSA-SAF meteosat second generation daily surface albedo (MDAL) retrieval algorithm incorporating aerosol correction and other improvements. *Geoscientific Instrumentation, Methods and Data Systems*, 11(2), 389–412. <https://doi.org/10.5194/gi-11-389-2022>
- Kharbouche, S., Song, R., & Muller, J.-P. (2019). Ground-based observations for validation (GBOV) of copernicus global land products: Algorithm theoretical basis document – energy products. Algorithm theoretical basis document, Copernicus/University College London.
- Lellouch, G., Carrer, D., Vincent, C., Pardé, M., Frietas, S., & Trigo, I. (2020). Evaluation of two global land surface albedo datasets distributed by the copernicus climate change service and the EUMETSAT LSA-SAF. *Remote Sensing*, 12(11), 1888. <https://doi.org/10.3390/rs12111888>
- Liu, Q., Wen, J., Qu, Y., He, T., Zhang, X., & Wang, L. (2012). *Broadband albedo*, pages 173–231.
- LSA-SAF. (2018a). *Algorithm theoretical basis document for Ten-day surface albedo from EPS/METOP/AVHRR (ETAL)*. Algorithm theoretical basis document. Meteo France/IPMA.
- LSA-SAF. (2018b). *Product user manual for land surface albedo*. Product User Manual.
- Moparthy, S., Carrer, D., & Ceamanos, X. (2019). Can we detect the brownness or greenness of the Congo rainforest using satellite-derived surface albedo? A study on the role of aerosol uncertainties. *Sustainability*, 11(5), 1410. <https://doi.org/10.3390/su11051410>
- Novick, K., & Phillips, R. (2022). AmeriFlux FLUXNET-1F US-MMS Morgan Monroe State Forest, Ver.
- Riihelä, A., Manninen, T., & Laine, V. (2013). Observed changes in the albedo of the Arctic sea-ice zone for the period 1982–2009. *Nature Climate Change*, 3(10), 895–898. <https://doi.org/10.1038/nclimate1963>
- Román, M., Schaaf, C., Woodcock, C., Strahler, A., Yang, X., Braswell, R., Curtis, P., Davis, K., Dragoni, D., & Goulden, M. (2009). The MODIS (collection v005) BRDF/albedo product: Assessment of spatial representativeness over forested landscapes. *Remote Sensing of Environment*, 113(11), 2476–2498. <https://doi.org/10.1016/j.rse.2009.07.009>
- Rougier, N. (2021). Scientific Visualization: Python + Matplotlib. 978-2-9579901-0-8. hal-03427242.
- Sánchez-Zapero, J., Camacho, F., Martínez-Sánchez, E., Lacaze, R., Carrer, D., Pinault, F., Benhadj, I., & Muñoz-Sabater, J. (2020). Quality assessment of PROBA-V surface albedo V1 for the continuity of the copernicus climate change service. *Remote Sensing*, 12(16), 2596. <https://doi.org/10.3390/rs12162596>
- Schaaf, C., Gao, F., Strahler, A., Lucht, W., Li, X., Tsang, T., Struggnell, N., Zhang, X., Jin, Y., Muller, J., Lewis, P., Barnsley, M., Hobson, P., Disney, M., Roberts, G., Dunderdale, M., Doll, C., d'Entremont, R. P. ... Privette, J. L. (2002). First operational BRDF, albedo nadir reflectance products from MODIS. *Remote Sensing of Environment*, 83(1–2), 135–148. [https://doi.org/10.1016/S0034-4257\(02\)00091-3](https://doi.org/10.1016/S0034-4257(02)00091-3)
- Schaepman-Strub, G., Schaepman, M., Painter, T., Dangel, S., & Martonchik, J. (2006). Reflectance quantities in optical remote sensing definitions and case studies. *Remote Sensing of Environment*, 103(1), 27–42. <https://doi.org/10.1016/j.rse.2006.03.002>
- USGS. (2020). Test sites catalog, https://calval.cr.usgs.gov/apps/test_sites_catalog.
- Vogt, R. (2021). Basic and other measurements of radiation at station Gobabeb.
- Vuilleumier, L. (2021). Developing a UV climatology for public health purposes using satellite data. *Environment International*, 146. <https://doi.org/10.1016/j.envint.2020.106177>
- Wang, Z., Schaaf, C., Lattanzio, A., Carrer, D., Grant, I., Román, M., Camacho, F., Yu, Y., Sánchez-Zapero, J., & Nickeson, J. (2019). Global Surface Albedo Product Validation Best Practices Protocol. Version 1.0. *Best Practice for Satellite Derived Land Product Validation*, 45. <https://doi.org/10.5067/DOC/CEOSWGCV/LPV/ALBEDO.0011>
- WMO. (2011). Systematic observation requirements for satellite-based data products for climate: Supplemental details to the satellite-based component of the 'implementation plan for the global observing system for climate in support of the UNFCCC (2010 update)'. Technical Report GCOS – 154.

Appendix A. Additional figures

Results for black-sky albedo (BSA).

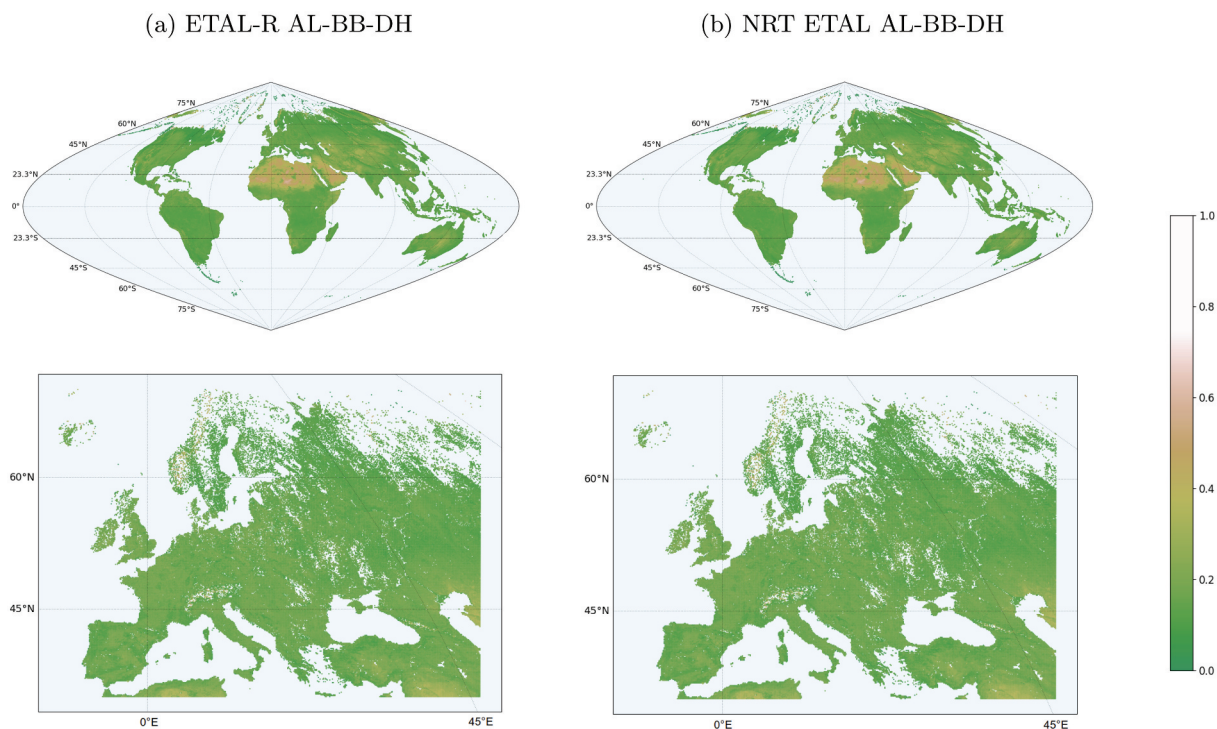


Figure A.1 - (a) ETAL-R and (b) NRT-generated ETAL AL-BB-DH on 5th June 2021, on a global scale and with a zoom on Europe.



Figure A.2 - Time series of MBE (red points) and STD (blue vertical lines) averaged for the full globe, for AL-BB-DH ≥ 0.15 (top) and < 0.15 (bottom).

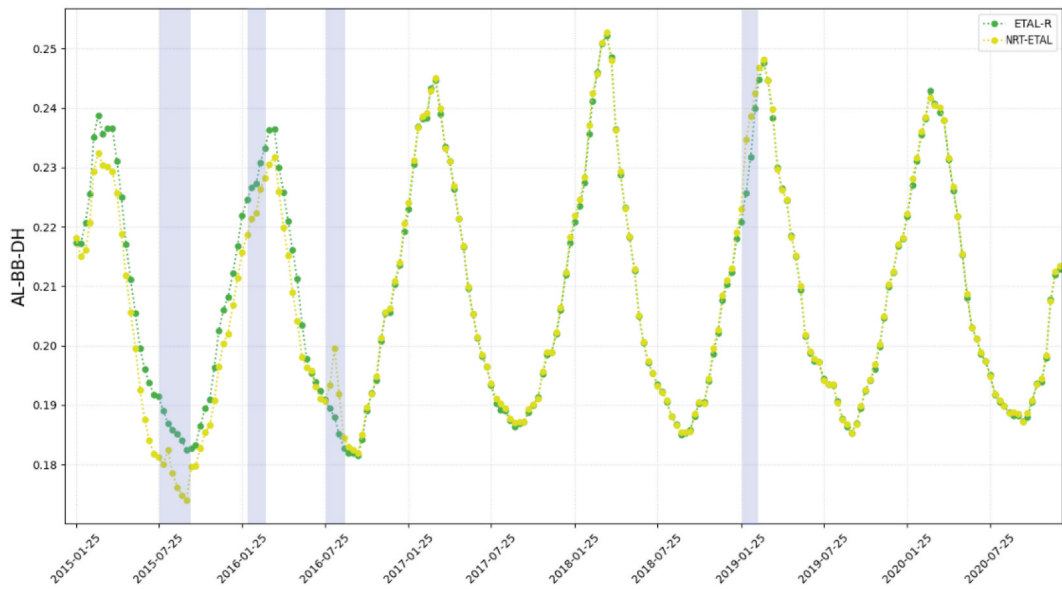


Figure A.3 - Time series of ETAL-R and NRT-generated ETAL AL-BB-DH averaged over the full globe with periods of anomalies (blue areas).

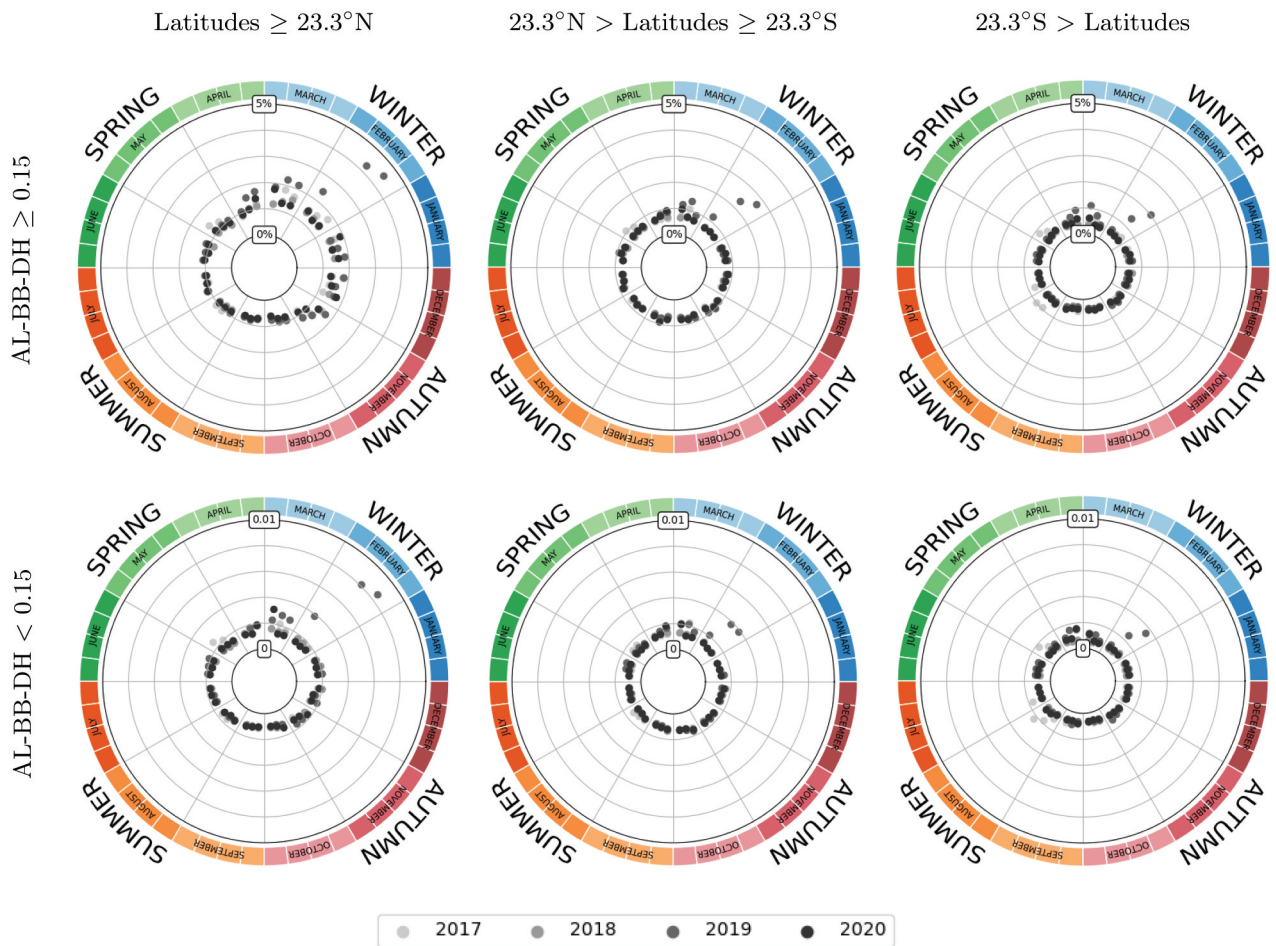


Figure A.4 - MAE score depending on latitudes, for $\text{AL-BB-DH} \geq 0.15$ and < 0.15 . The seasons correspond to the Northern Hemisphere. Figure was made using scripts from Rougier (2021).

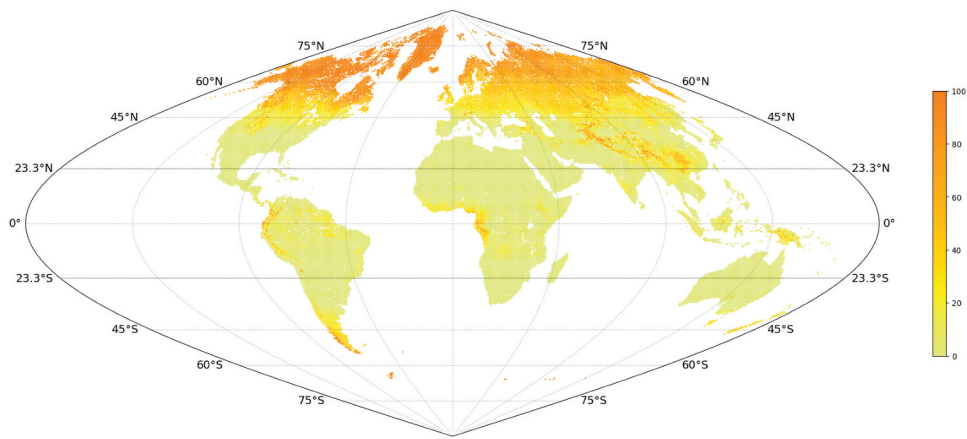


Figure A.5 - Percentage of missing data for ETAL-R AL-BB-DH averaged over 2020.

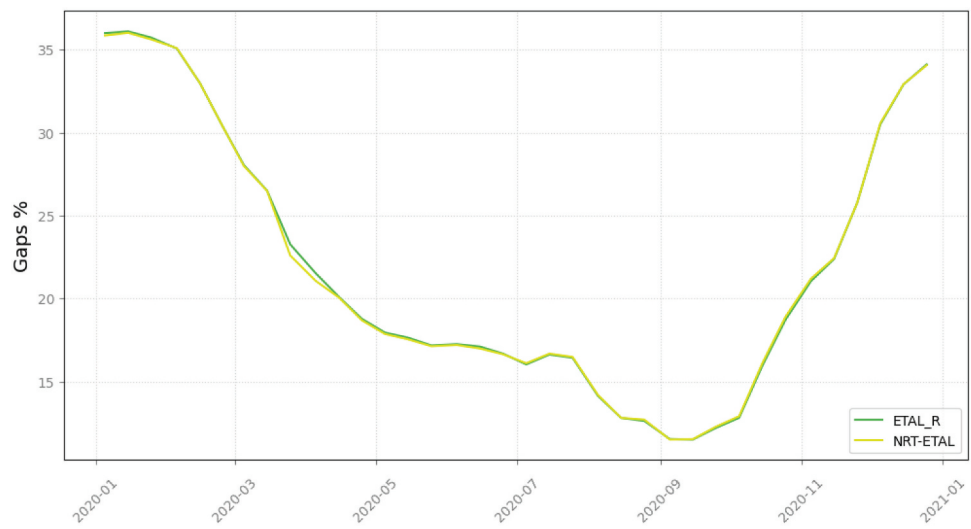
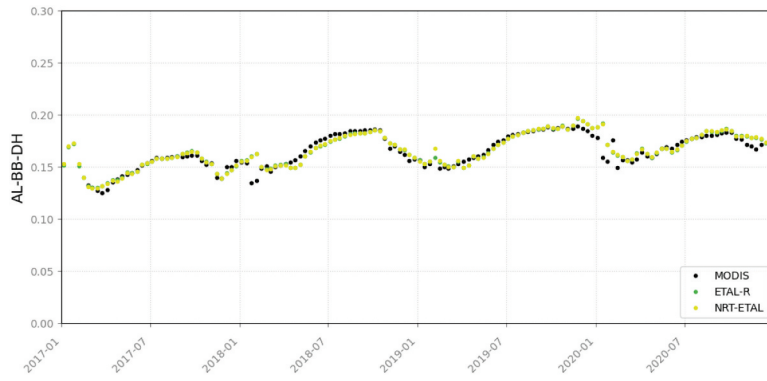


Figure A.6 - Percentage of missing data for ETAL-R and NRT ETAL AL-BB-DH averaged over the globe for 2020.



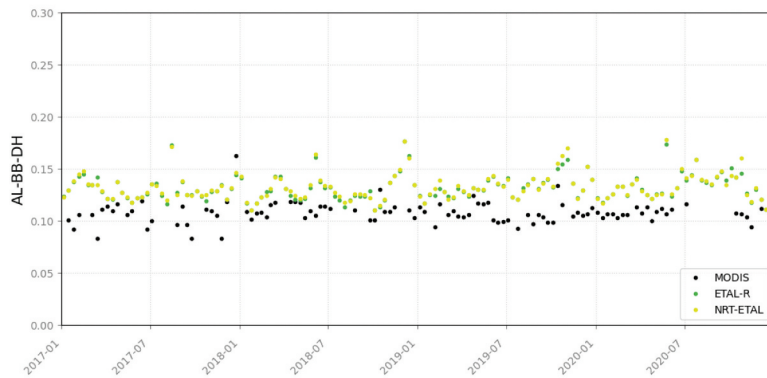
Figure A.7 - Time series of ETAL-R and near-real time generated ETAL AL-BB-DH surface albedo 3×3 pixels area with various scores for both 3×3 and 5×5 pixels area. Dashed lines represent the mean of the time series and dotted lines the temporal standard deviation. First two years are grayed out because they were not considered in the calculation of the scores due to the convergence phase of ETAL-R.

(a) Australia



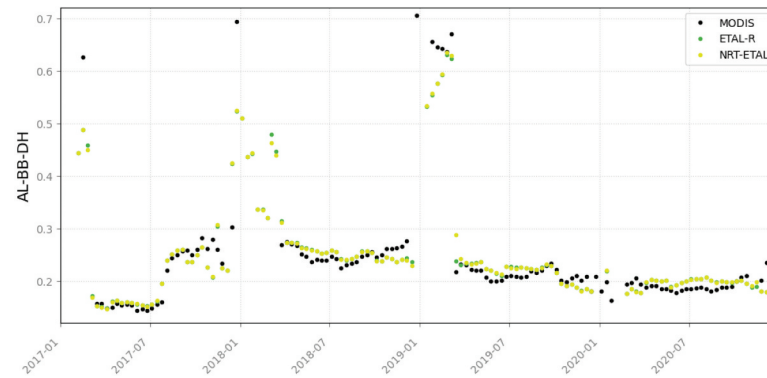
	ETAL-R	NRT-ETAL
MedAE	1.5 %	1.4 %
MBE	0.4 %	0.4 %
MAE	2.0 %	2.0 %
RMSD	10.8 %	10.4 %
N	112	112
R	0.92	0.92

(b) Democratic Republic of the Congo



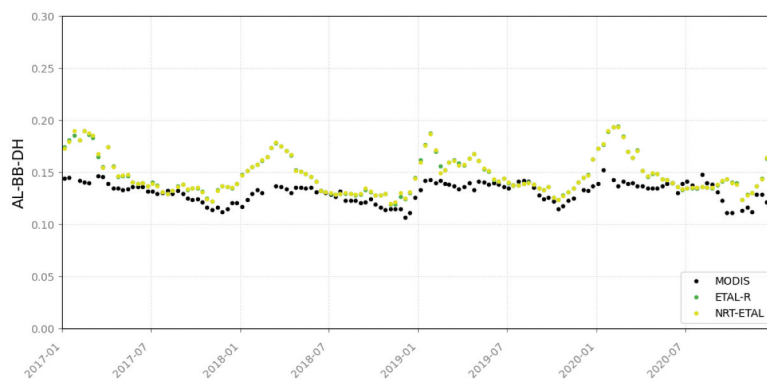
	ETAL-R	NRT-ETAL
MedAE	0.023	0.022
MBE	0.023	0.024
MAE	0.024	0.024
RMSD	0.023	0.023
N	101	101
R	0.03	0.10

(c) Kazakhstan



	ETAL-R	NRT-ETAL
MedAE	6.4 %	6.4 %
MBE	1.1 %	1.3 %
MAE	7.4 %	7.6 %
RMSD	6.6 %	6.7 %
N	111	111
R	0.96	0.96

(d) Mozambique



	ETAL-R	NRT-ETAL
MedAE	0.012	0.012
MBE	0.015	0.015
MAE	0.016	0.016
RMSD	0.020	0.020
N	136	136
R	0.62	0.62

Figure A.8 - Time series of ETAL-R and NRT-generated ETAL AL-BB-DH compared to MODIS with statistics scores.

Appendix B. Metrics

v : set of observations to assess

μ : average of v

v_r : set of reference values

μ_r : average of v_r

Mean Bias Error

$$MBE = \frac{1}{n} \sum_{i=1}^n (v - v_r) \quad (1)$$

Relative Mean Bias Error

$$MBEr = \frac{MBE}{\mu_r} \times 100 \quad (1)$$

Mean Absolute Error

$$MAE = \frac{1}{n} \sum_{i=1}^n |v - v_r| \quad (1)$$

Relative Mean Absolute Error

$$MAEr = \frac{MAE}{\mu_r} \times 100 \quad (1)$$

Median Absolute Error

$$MedAE = \text{median}(|v - v_1|, \dots, |v - v_r|) \quad (1)$$

Relative Median Absolute Error

$$MedAEr = \frac{MedAE}{\mu_r} \times 100 \quad (1)$$

Root Mean Square Deviation

$$RMSD = \sqrt{\frac{1}{n} \sum_{i=1}^n (v - v_r)^2} \quad (1)$$

Relative Root Mean Square Deviation

$$RMSDr = \frac{RMSD}{v_{r_{max}} - v_{r_{min}}} \times 100 \quad (1)$$

Pearson's correlation coefficient R

$$R = \frac{\sum_{i=1}^n (v - \mu)(v_r - \mu_r)}{\sqrt{\sum_{i=1}^n (v - \mu)^2 \sum_{i=1}^n (v_r - \mu_r)^2}} \quad (1)$$

Standard Deviation

$$STD = \sqrt{\frac{1}{n} \sum_{i=1}^n v^2 - \mu^2} \quad (1)$$

Standard Deviation Relative to Mean

$$STD_r = \frac{STD}{\mu} \times 100 \quad (1)$$

Appendix C. Glossary

AL:	Land Surface <u>A</u> lbedo <u>P</u> roduct
AVHRR:	<u>A</u> dvanced <u>V</u> ery <u>H</u> igh <u>R</u> esolution <u>R</u> adiometer
BB:	<u>B</u> road- <u>b</u> and
BH:	<u>B</u> i-hemispherical
BRDF:	<u>B</u> i-directional <u>R</u> eflectance <u>D</u> istribution <u>F</u> unction
BSA:	<u>B</u> lack <u>S</u> ky <u>A</u> lbedo
BSRN:	<u>B</u> aseline <u>S</u> urface <u>R</u> adiation <u>N</u> etwork
CEOS:	<u>C</u> ommittee on <u>E</u> arth <u>O</u> bservation <u>S</u> atellites
CGMS:	<u>C</u> oordination <u>G</u> roup for <u>M</u> eteorological <u>S</u> atellite
CMG:	<u>C</u> limate <u>M</u> odeling <u>G</u> rid
CNRM:	<u>C</u> entre <u>N</u> ational de <u>R</u> echerches <u>M</u> étéorologiques
DH:	<u>D</u> irectional-hemispherical
ECMWF:	<u>E</u> uropean <u>C</u> entre for <u>M</u> edium- <u>R</u> ange <u>W</u> eather <u>F</u> orecast
ECV:	<u>E</u> ssential <u>C</u> limate <u>V</u> ariables
EPS:	<u>E</u> UMETSAT <u>P</u> olar <u>S</u> ystem
ERAS:	<u>F</u> ifth <u>G</u> eneration of <u>E</u> CMWF <u>A</u> tmospheric <u>R</u> eanalysis
ETAL:	<u>E</u> PS <u>T</u> en-day <u>S</u> urface <u>A</u> lbedo
ETAL-R:	<u>ETAL</u> reprocessing
EUMETSAT:	<u>E</u> uropean <u>M</u> eteorological <u>S</u> atellite <u>O</u> rganisation
FAPAR:	<u>F</u> raction of <u>A</u> bsorbed <u>P</u> hotosynthetically <u>A</u> ctive <u>R</u> adiation
GBOV:	<u>G</u> round- <u>B</u> ased <u>O</u> bservations for <u>V</u> alidation of <u>C</u> opernicus <u>G</u> lobal <u>L</u> and <u>P</u> roducts
GCOS:	<u>G</u> lobal <u>C</u> limate <u>O</u> bserving <u>S</u> ystem
GPM:	<u>G</u> lobal <u>P</u> recipitation <u>M</u> easurement
HDF5:	<u>H</u> ierarchical <u>D</u> ata <u>F</u> ormat <u>5</u>
IGBP:	<u>I</u> nternational <u>G</u> eosphere- <u>B</u> iosphere <u>P</u> rogramme
IMERG:	<u>I</u> ntegrated <u>M</u> ulti-satellit <u>E</u> <u>R</u> etrievals for <u>G</u> PM
IPMA:	<u>I</u> nstituto <u>P</u> ortuguês do <u>M</u> ar e da <u>A</u> tmosfera (Portugal)
LAI:	<u>L</u> eaf <u>A</u> rea <u>I</u> ndex
LP DAAC:	<u>L</u> and <u>P</u> rocesses <u>D</u> istributed <u>A</u> ctive <u>A</u> rchive <u>C</u> enter
LSA:	<u>L</u> and <u>S</u> urface <u>A</u> nalysis
MDAL:	<u>M</u> SG <u>D</u> aily <u>S</u> urface <u>A</u> lbedo
METEOSAT:	<u>G</u> eostationary <u>M</u> eteorological <u>S</u> atellite
METOP:	<u>M</u> eteorological <u>O</u> perational <u>P</u> olar <u>S</u> atellites of <u>E</u> UMETSAT
MF:	<u>M</u> étéo- <u>F</u> rance
MODIS:	<u>M</u> odderate- <u>R</u> esolution <u>I</u> maging <u>S</u> pectro- <u>R</u> adiometer
MSG:	<u>M</u> eteosat <u>S</u> econd <u>G</u> eneration
NASA:	<u>N</u> ational <u>A</u> eronautics and <u>S</u> pace <u>A</u> dmistration
NB:	<u>N</u> arrow- <u>b</u> and
NDVI:	<u>N</u> ormalized <u>D</u> ifference <u>V</u> egetation <u>I</u> ndex
NetCDF4:	<u>N</u> etwork <u>C</u> ommon <u>D</u> ata <u>F</u> orm
NIR:	<u>N</u> ear <u>i</u> nfrared
NRT:	<u>N</u> ear <u>R</u> eal <u>T</u> ime
NWP:	<u>N</u> umerical <u>W</u> eather <u>P</u> rediction
PRD:	<u>P</u> roduct <u>R</u> equirements <u>D</u> ocument
PROBA-V:	<u>P</u> roject for <u>O</u> n- <u>B</u> oard <u>A</u> utonomy <u>V</u> egetation
SAVS:	<u>S</u> urface <u>A</u> lbedo <u>V</u> alidation <u>S</u> ites
SAF:	<u>S</u> atellite <u>A</u> pplication <u>F</u> acility
SEVIRI:	<u>S</u> pinning <u>E</u> nhanced <u>V</u> isible and <u>I</u> nfrared <u>I</u> mager
SWD:	<u>S</u> hortwave <u>d</u> own- <u>w</u> elling
SWU:	<u>S</u> hortwave <u>u</u> p- <u>w</u> elling
TOC:	<u>T</u> op of <u>C</u> anopy
TOA:	<u>T</u> op of <u>A</u> tmosphere
USGS:	<u>U</u> nited <u>S</u> tates <u>G</u> eological <u>S</u> urvey
VIS:	<u>V</u> isible
WMO:	<u>W</u> orld <u>M</u> eteorological <u>O</u> rganization
WSA:	<u>W</u> hite <u>S</u> ky <u>A</u> lbedo
